



**HAL**  
open science

## A single MYB transcription factor with multiple functions during flower development

Mathilde Chopy, Marta Binaghi, Gina Cannarozzi, Rayko Halitschke, Benoît Boachon, Roel Heutink, Dikki Pedenla Bomzan, Lea Jäggi, Geert van Geest, Julian Verdonk, et al.

### ► To cite this version:

Mathilde Chopy, Marta Binaghi, Gina Cannarozzi, Rayko Halitschke, Benoît Boachon, et al.. A single MYB transcription factor with multiple functions during flower development. *New Phytologist*, 2023, 239 (5), pp.2007-2025. 10.1111/nph.19096 . hal-04704330

**HAL Id: hal-04704330**

**<https://hal.science/hal-04704330v1>**

Submitted on 20 Sep 2024

**HAL** is a multi-disciplinary open access archive for the deposit and dissemination of scientific research documents, whether they are published or not. The documents may come from teaching and research institutions in France or abroad, or from public or private research centers.

L'archive ouverte pluridisciplinaire **HAL**, est destinée au dépôt et à la diffusion de documents scientifiques de niveau recherche, publiés ou non, émanant des établissements d'enseignement et de recherche français ou étrangers, des laboratoires publics ou privés.



Distributed under a Creative Commons Attribution 4.0 International License

1 **A single MYB transcription factor with multiple functions during flower development**

2  
3 Mathilde Chopy<sup>1</sup>, Marta Binaghi<sup>1</sup>, Gina Cannarozzi<sup>1</sup>, Rayko Halitschke<sup>2</sup>, Benoît Boachon<sup>3</sup>, Roel  
4 Heutink<sup>4</sup>, Dikki Pedenla Bomzan<sup>3</sup>, Lea Jäggi<sup>1</sup>, Geert van Geest<sup>5</sup>, Julian C. Verdonk<sup>4</sup> and Cris  
5 Kuhlemeier<sup>1</sup>

6  
7 <sup>1</sup>Institute of Plant Sciences, University of Bern, Altenbergrain 21, 3013 Bern, Switzerland;  
8 <sup>2</sup>Department of Mass Spectrometry and Metabolomics, Max-Planck-Institute for Chemical  
9 Ecology, Hans-Knöll-Str. 8, 07745 Jena, Germany; <sup>3</sup>Université Jean Monnet Saint-Etienne,  
10 CNRS, LBVpam UMR 5079, F-42023, Saint-Etienne, France ; <sup>4</sup>Horticulture and Product  
11 Physiology, Plant Science Group, Wageningen University and Research, 6708 Wageningen,  
12 Netherlands; <sup>5</sup>Interfaculty Bioinformatics Unit, University of Bern, Baltzerstrasse 6, 3012 Bern,  
13 Switzerland

14  
15 ORCID details for authors:

16  
17 **Mathilde Chopy**

18 Email: mathilde.chopy@unibe.ch

19 ORCID: 0000-0003-4403-5769

20 Affiliation: Institute of Plant Sciences, University of Bern, Altenbergrain 21, 3013 Bern,  
21 Switzerland

22 Twitter: @MathildeChopy

23  
24 **Marta Binaghi**

25 Email: marta.binaghi@unibe.ch

26 ORCID: 0000-0001-6951-792X

27 Affiliation: Institute of Plant Sciences, University of Bern, Altenbergrain 21, 3013 Bern,  
28 Switzerland

29 Twitter: @martabinaghi

30  
31 **Gina Cannarozzi**

32 Email: cannarozzi@chem.ethz.ch

33 ORCID: 0000-0002-0704-663X

34 Affiliation: Institute of Plant Sciences, University of Bern, Altenbergrain 21, 3013 Bern,  
35 Switzerland

36 Twitter: @GinaCannarozzi

37

38 **Rayko Halitschke**

39 Email: rhalitschke@ice.mpg.de

40 ORCID: 0000-0002-1109-8782

41 Affiliation: Department of Mass Spectrometry and Metabolomics, Max-Planck-Institute for  
42 Chemical Ecology, Hans-Knöll-Str. 8, 07745 Jena, Germany

43

44 **Benoît Boachon**

45 Email: benoit.boachon@univ-st-etienne.fr

46 ORCID: 0000-0002-2362-2238

47 Affiliation: Université Jean Monnet Saint-Etienne, CNRS, LBVpam UMR 5079, F-42023, Saint-  
48 Etienne, France

49 Twitter: @BB\_VOCsPoP

50

51 **Roel Heutink**

52 Email: roel.heutink@wur.nl

53 ORCID: 0000-0002-6084-2395

54 Affiliation: Horticulture and Product Physiology, Plant Science Group, Wageningen University  
55 and Research, 6708 Wageningen, Netherlands

56

57 **Dikki Pedenla Bomzan**

58 Email: dikki.pedenla.bomzan@univ-st-etienne.fr

59 ORCID: 0000-0003-0595-0569

60 Affiliation: Université Jean Monnet Saint-Etienne, CNRS, LBVpam UMR 5079, F-42023, Saint-  
61 Etienne, France

62

63 **Lea Jäggi**

64 Email: lea.jaeggi@unibe.ch

65 ORCID: no ORCID number

66 Affiliation : Institute of Plant Sciences, University of Bern, Altenbergrain 21, 3013 Bern,  
67 Switzerland

68

69 **Geert van Geest**

70 Email: geert.vangeest@unibe.ch

71 ORCID: 0000-0002-1561-078X

72 Affiliation: Interfaculty Bioinformatics Unit, University of Bern, Baltzerstrasse 6, 3012 Bern,  
73 Switzerland

74 Twitter: @geertvangeest

75

76 **Julian Verdonk**

77 Email: julian.verdonk@wur.nl

78 ORCID: 0000-0002-1237-7951

79 Affiliation: Horticulture and Product Physiology, Plant Science Group, Wageningen University  
80 and Research, 6708 Wageningen, Netherlands

81 Twitter: @JulianVerdonk

82

83 **Cris Kuhlemeier**

84 Email: cris.kuhlemeier@unibe.ch

85 ORCID: 0000-0003-2440-5937

86 Affiliation: Institute of Plant Sciences, University of Bern, Altenbergrain 21, 3013 Bern,  
87 Switzerland

88

89 Author for correspondence:

90 *Cris Kuhlemeier*

91 *Tel: 031 3510317 or 077 4359223*

92 *Email: [cris.kuhlemeier@ips.unibe.ch](mailto:cris.kuhlemeier@ips.unibe.ch)*

93

94



95 **SUMMARY**

- 96 • Members of the R2R3-MYB transcription factor subgroup 19 (SG19) have been  
97 extensively studied in multiple plant species using different silenced or mutated lines.  
98 Some studies have proposed a function in flower opening, others in floral organ  
99 development/maturation, or specialized metabolism production. While SG19 members are  
100 clearly key players during flower development and maturation, the resulting picture is  
101 complex, confusing our understanding in how SG19 genes function.
- 102 • To clarify the function of the SG19 transcription factors, we used a single system, *Petunia*  
103 *axillaris*, and targeted its two SG19 members (*EOB1* and *EOB2*) by CRISPR-Cas9.
- 104 • Although *EOB1* and *EOB2* are highly similar, they display radically different mutant  
105 phenotypes. *EOB1* has a specific role in scent emission while *EOB2* has pleiotropic  
106 functions during flower development. The *eob2* knockout mutants reveal that *EOB2* is a  
107 repressor of flower bud senescence by inhibiting ethylene production. Moreover, partial  
108 loss-of-function mutants (transcriptional activation domain missing) show that *EOB2* is  
109 also involved in both petal and pistil maturation through regulation of primary and  
110 secondary metabolism.
- 111 • Here we provide new insights into the genetic regulation of flower maturation and  
112 senescence. It also emphasizes the function of *EOB2* in the adaptation of plants to specific  
113 guilds of pollinators.

114

115 **KEY WORDS**

116 Flower development, flower maturation, *Petunia*, R2R3-MYB transcription factors, senescence,  
117 starch metabolism, terpenoids/isoprenoids/carotenoids, volatile compounds

118 **INTRODUCTION**

119 Flower development can be divided into floral organ identity establishment, growth, maturation,  
120 and senescence. Organ identity is established by the combinatorial action of the ABC class genes  
121 (Coen & Meyerowitz, 1991), and how it varies between species has been studied in detail (Soltis  
122 *et al.*, 2007). Once established, the organs grow out and differentiate to carry out their specific  
123 functions in pollinator attraction and reward. After pollination, petals and stamens senesce and  
124 seeds are produced within the ovary. Members of subgroup 19 (SG19) of the R2R3-MYB  
125 transcription factor family are key players in the later stages of floral organ development and  
126 maturation. A number of studies, mainly in Solanaceae and Arabidopsis, have documented their  
127 functions in flower opening (Colquhoun *et al.*, 2011; Reeves *et al.*, 2012; Liu & Thornburg,  
128 2012; Niwa *et al.*, 2018; Schubert *et al.*, 2019), senescence (Colquhoun *et al.*, 2011), nectary  
129 development (Liu *et al.*, 2009; Liu & Thornburg, 2012; Schmitt *et al.*, 2018), stamen  
130 development (Mandaokar *et al.*, 2006; Cheng *et al.*, 2009; Song *et al.*, 2011; Reeves *et al.*, 2012;  
131 Qi *et al.*, 2015; Huang *et al.*, 2017; Battat *et al.*, 2019; Huang *et al.*, 2020), ovule fertility  
132 (Schubert *et al.*, 2019), pistil length (Reeves *et al.*, 2012; Schubert *et al.*, 2019; Yarahmadov *et al.*,  
133 2020), as well as production of secondary metabolites such as scent compounds (Spitzer-  
134 Rimon *et al.*, 2010, 2012; Van Moerkercke *et al.*, 2012; Medina-Puche *et al.*, 2015; Ke *et al.*,  
135 2021), flavonols or terpenes (Battat *et al.*, 2019; Shan *et al.*, 2020; Yang *et al.*, 2020; Zhang *et al.*,  
136 2021b,a) (**Fig. 1a**). These later stages have been studied in a variety of species, often with a  
137 variety of molecular tools. Consequently, it is often not clear whether contrasting mutant  
138 phenotypes are species-specific, or are due to the methods used, to the focus of the study on a  
139 particular organ, or to the multi-functionality of the SG19 MYB factors. For example, RNAi lines  
140 targeting tobacco *MYB305* led to nectary maturation defects in one study (Liu *et al.*, 2009; Liu &  
141 Thornburg, 2012), and to flower opening defects in another study (Colquhoun *et al.*, 2011).  
142 Different phenotypes were also observed in *Petunia hybrida*, where targeting *EOB2* by VIGS  
143 exclusively affected scent production (Spitzer-Rimon *et al.*, 2010) whereas RNAi caused flower  
144 opening defects (Colquhoun *et al.*, 2011).

145

146 The R2R3-MYB SG19 transcription factors are characterized by two main functional domains:  
147 an R2R3-MYB domain (RMD<sup>SG19</sup>) located at the N-terminus and a transcriptional activation  
148 domain (TAD) located at the C-terminus (Liu *et al.*, 2009; Schubert *et al.*, 2019; Wu *et al.*,  
149 2021b) (**Fig. 1b**). The RMD<sup>SG19</sup> and the TAD molecular functions have been individually

150 characterized using different experimental and computational techniques. In summary, the  
151 RMD<sup>SG19</sup> has at least three roles: (1) interact with different proteins (bHLHs, JAZs, DELLAs,...)  
152 (Song *et al.*, 2011; Qi *et al.*, 2015; Huang *et al.*, 2017; Liu *et al.*, 2017; Schubert *et al.*, 2019;  
153 Huang *et al.*, 2020; Yang *et al.*, 2020; Ke *et al.*, 2021; Zhang *et al.*, 2021b) , (2) bind DNA  
154 through the recognition of particular cis-element targets ([G/A]TT[A/T]GG[T/C]) (Weirauch *et al.*,  
155 2014; Medina-Puche *et al.*, 2015), and (3) reach the nucleus through the nuclear localization  
156 signal (NLS) (Liu *et al.*, 2009). On the other hand, the TAD recruits the transcriptional machinery  
157 and through synergic action, the TAD and RMD, regulate the expression of a wide range of  
158 targets (Sablowski *et al.*, 1994; Moyano *et al.*, 1996; Liu *et al.*, 2009; Spitzer-Rimon *et al.*, 2010;  
159 Liu & Thornburg, 2012; Moerkercke *et al.*, 2011; Medina-Puche *et al.*, 2015; Battat *et al.*, 2019;  
160 Kurilla *et al.*, 2019; Yang *et al.*, 2020; Bian *et al.*, 2021; Zhang *et al.*, 2021b; Wu *et al.*, 2021b;  
161 Ke *et al.*, 2021; Zhang *et al.*, 2021a; Wang *et al.*, 2022) (**Tables S1, S2**). R2R3-MYB SG19  
162 protein sequences have the typical features of transcriptional activators. No characteristic  
163 repression motifs (EAR or TLLRF) (Ma & Constabel, 2019) were found and all the targets  
164 identified in the literature (except one) were directly activated by R2R3-MYB SG19 members  
165 (**Table S2**). According to these results, SG19 members associate with a plethora of interacting  
166 proteins and promoters providing the potential to regulate many different processes of flower  
167 development.

168  
169 The complex and conflicting data on the function of SG19s during flower development  
170 necessitates an in-depth structural and functional characterization of its members. To do so, we  
171 used a single system, *P. axillaris*, where two members of the SG19 clade have been identified:  
172 EMISSION OF BENZENOIDES I and II (EOB1 and EOB2). Those two genes have a flower-  
173 specific expression pattern. We generated mutations in *EOB1* and *EOB2* using CRISPR-Cas9,  
174 and analyzed their different functions. Domain-mutants also reveal the specific contributions of  
175 the two domains, RMD<sup>SG19</sup> and TAD, in EOB2 functions. These discoveries made it clear that  
176 EOB2 is a complex multi-functional protein during floral organ development. Our study  
177 contributes to explain the complexity of the R2R2-MYB SG19 associated functions observed  
178 within and between species and in a broader perspective to study flower maturation.

179

## 180 MATERIALS AND METHODS

181

182 **Plant material and growth conditions**

183 *Petunia axillaris* (Lam.) *ssp. axillaris* P (referred to as *P. ax* P or WT) originates from the  
184 University of Bern Botanical Garden (Hoballah *et al.*, 2005). Plants were grown in a growth  
185 chamber under a light : dark regime of 15 h : 9 h at 22°C : 17°C, in commercial soil (70%  
186 Klasman substrate, 15% Seramis clay granules, 15% quartz sand), and fertilized once a week  
187 with a nitrogen-phosphorous-potassium and iron fertilizer.

188  
189 **Generation of phylogenetic tree**

190 Phylogenetic reconstruction focused on R2R3-MYB subgroup 19 from *Arabidopsis thaliana* (*At*),  
191 *Solanum lycopersicum* (*Sl*), *Nicotiana tabacum* (*Nt*), *Petunia hybrida* (*Ph*) and *Petunia axillaris*  
192 (*Pax*). Protein sequences alignment was performed with the plug-in version of MUSCLE for  
193 UGENE, version 40.1, default parameters (Edgar, 2004; Okonechnikov *et al.*, 2012). Tree was  
194 built with PhyML version 20120412 in UGENE, with LG substitution matrix, branch support  
195 calculated with SH-like method (Guindon *et al.*, 2010).

196  
197 **Vectors construction**

198 The CRISPR-Cas9 Vectors (pHSE401, dual gRNA), called VB191229-3063hgg and VB190510-  
199 1037erq targeting *EOB1* or *EOB2* respectively, were commercially synthesized by VectorBuilder  
200 (<https://en.vectorbuilder.com/design/retrieve.html>). For each vector, two unique gRNAs were  
201 selected (gRNA sequences are listed in **Table S3**).

202  
203 ***Petunia axillaris* P stable transformation with Agrobacterium**

204 Stable transformation procedure is based on a classical transformation protocol (Chopy *et al.*,  
205 2020) with some modifications. Briefly, leaves from 4-6 week old plants of *P. axillaris* P were  
206 surface sterilized and cut with a scalpel blade into one cm<sup>2</sup> small pieces. Sterilized leaf disks were  
207 put in a liquid *A. tumefaciens* (strain LBA4404) suspension for 30 minutes, dried between two  
208 layers of sterile filter papers and transferred to a co-culture plate medium for 5 days at 24°C (in  
209 the dark with a progressive increase of light). Then, once a week, leaf fragments were transferred  
210 to a fresh selective medium containing the appropriate selection agent and were kept at 24°C with  
211 moderate light, under long day conditions until the apparition of shoots. Each individual shoot  
212 was excised from the calli and transferred to a rooting medium. After rooting, plants were

213 transplanted to soil and grown in a growth chamber. The screening was then performed on these  
214 plants after one week to allow them to acclimatize to the soil conditions.

215

### 216 **Overexpression constructs and transient expression**

217 The full-length cDNAs of *EOB1*, *EOB2*, *eob2-2* and *eob2-3* from *P. axillaris* wild-type, *eob2-2*  
218 or *eob2-3* were cloned (**Table S4**) in the pDONR221 vector (Invitrogen) and transferred to the  
219 pGWB402 vector (NAKAGAWA *et al.*, 2007). Transient transformation of *Petunia axillaris* P  
220 leaves using *A. tumefaciens* (strain GV3101) was performed as in (Moerkercke *et al.*, 2011) with  
221 some modifications. *Petunia* leaves from 4-6 week old plants were syringe-infiltrated. Three days  
222 later, four replicates per construct were harvested (one replicate consists of 3 leaf disks of 8 mm  
223 of diameter near to the agroinfiltrated position) and RT-qPCR were performed using *RAN1* as  
224 reference gene.

225

### 226 **DNA extraction and genotyping**

227 Genomic DNA was extracted from fresh leaf samples using a modified SDS extraction protocol  
228 (Edwards *et al.*, 1991). Primer pairs used for the genotyping are listed in **Table S4**.

229

### 230 **Color images**

231 Flower and branch images were recorded with a Canon EOS 60D camera and Canon 35 mm lens.  
232 Floral organ pictures were photographed under a stereoscopic microscope (Nikon, SMZ1500)  
233 equipped with a camera (Leica, DMC6200)

234

### 235 **Phenotypic measurements**

236 Before phenotyping, the *eob1* or *eob2* single homozygous mutants or heterozygous lines, cas9-  
237 negative lines were selected and we confirmed by sequencing that our gRNAs specifically  
238 targeted either *EOB1* or *EOB2*. Phenotypic measurements included tube length, opening angle,  
239 limb area, nectar volume and scent emission. All the flowers used for phenotyping were  
240 harvested one day post anthesis right before the onset of dark in the growth chamber.  
241 Petal morphological traits (tube length, opening angle, limb area) were measured by  
242 photographing front and side view of 12 flowers per genotype. Images were analyzed using the  
243 ImageJ software. Nectar volumes were quantified according to the protocol described in  
244 (Brandenburg *et al.*, 2012). Methylbenzoate and benzaldehyde compounds were analyzed as

245 described previously by proton transfer reaction mass spectrometry (PTR-MS, Ionicon®) (Amrad  
246 *et al.*, 2016). Five flowers per plant were analyzed as biological replicates.

247

### 248 **RNA extractions, cDNA preparation and quantitative RT-PCR**

249 The different tissue samples used in this study were collected in three biological replicates and  
250 stored at -80°C until further processing. RNA extractions were performed using an innuPREP  
251 DNA/RNA Mini Kit (Analytik Jena; code 845-KS-20800250). cDNA was synthesized using the  
252 qScriber cDNA synthesis kit (HighQu; code RTK0104) and for RT-qPCR the ORA SEE qPCR  
253 Green ROX L mix (HighQu; code QPD0505) was used according to the manufacturer's  
254 recommendations. The amplification was performed using a QuantStudio 5 Real-Time PCR  
255 Instrument 346 (Applied Biosystems). The reference genes used to analyze the data  
256 were *RANI* and *ACTIN11* (Mallona *et al.*, 2010). Primer pairs are listed in **Table S4**.

257

### 258 **RNA sequencing**

259 Total RNA was isolated from tissues listed in **Table S5** using an innuPREP DNA/RNA Mini Kit  
260 (Analytik Jena; code: 845-KS-20800250). The quantity and quality of the purified total RNA was  
261 assessed using a Thermo Fisher Scientific Qubit 4.0 fluorometer with the Qubit RNA BR Assay  
262 Kit (Thermo Fisher Scientific, Q10211) and an Advanced Analytical Fragment Analyzer System  
263 using a Fragment Analyzer RNA Kit (Agilent, DNF-471), respectively. Sequencing libraries  
264 were made using an Illumina TruSeq Stranded mRNA Library Prep kit (Illumina, 20020595) in  
265 combination with TruSeq RNA UD Indexes (Illumina, 20022371) according to Illumina's  
266 guidelines. Pooled cDNA libraries were sequenced paired-end using a shared Illumina NovaSeq  
267 6000 S1 Reagent Kit (200 cycles; Illumina, 20028318) on an Illumina NovaSeq 6000 instrument.  
268 The run produced a minimum of 36 million reads/sample. The quality of the sequencing run was  
269 assessed using Illumina Sequencing Analysis Viewer (Illumina version 2.4.7) and all base call  
270 files were demultiplexed and converted into FASTQ files using Illumina bcl2fastq conversion  
271 software v2.20. The quality control assessments, generation of libraries and sequencing were  
272 conducted by the Next Generation Sequencing Platform, University of Bern.

273

### 274 **Reads processing, differential expression analysis and GO**

275 The quality of the RNA-seq reads was assessed using fastqc v0.11.9 (Andrews, 2022). Adapters  
276 were trimmed with Cutadapt v3.4.1 (Martin, 2011). The reads were aligned to the *Petunia*

277 *axillaris* N reference genome version 4.03 (Peax403; available on NCBI GenBank under the  
278 accession GCA\_026929995.1) using hisat2 v2.2.1 (Kim *et al.*, 2015). FeatureCounts v2.0.1 (Liao  
279 *et al.*, 2014) was used to count the number of reads overlapping with each gene as specified in the  
280 genome annotation corresponding with Peax403 (gff file can be downloaded from CoGe with the  
281 id 62433). The Bioconductor package DESeq2 v1.36.0 (Love *et al.*, 2014) was used to test for  
282 differential gene expression between the experimental groups. Gene GO-term mappings were  
283 obtained from (Patrick *et al.*, 2021), and GO-term enrichment was performed with clusterProfiler  
284 v4.4.4 (Wu *et al.*, 2021a).

285

### 286 **1-MCP treatment**

287 To inhibit ethylene perception, WT, *eob2-1<sup>KO</sup>*, *eob2-2<sup>KO</sup>* and *eob2-3<sup>LofTAD</sup>* plants were placed in a  
288 growth chamber (Percival, model: E-36L2) and treated with an ethylene receptor antagonist, 1-  
289 MCP (1-methylcyclopropene) volatile treatment. To treat the plants two EthylBloc™ Sachets of  
290 2.5 grams (AgroFresh) were used and replaced once a day during at least two weeks.

291

### 292 **Ethylene measurements**

293 Ethylene measurements were performed using a laser-based photoacoustic ethylene sensor (ETD-  
294 300, SensorSense, Nijmegen, Netherlands). For WT and *eob2-1<sup>KO</sup>* ethylene measurements, full  
295 flower buds, dissected petals or pistils at stage 5 were used (three flowers per plant were analyzed  
296 as biological replicates, for WT n = 30 and for *eob2-1<sup>KO</sup>* n = 45). Mutant samples were collected  
297 before the first signs of senescence, when the petal tips were still rigid. Flower buds or dissected  
298 organs were enclosed in 4-mL vials and an accumulation time of 5 hours was used between  
299 harvest time and measurements. Ethylene concentrations were analyzed with a flow rate of 2.5 L  
300 h<sup>-1</sup> and quantified by signal integration after curve fitting. Ethylene concentrations were  
301 calculated based on measurements of a 500-ppb ethylene gas standard analyzed as a reference  
302 sample.

303

### 304 **Quantification of sesquiterpene accumulation in *Petunia* pistils and emission from tube**

305 Experiments were essentially performed as previously described (Boachon *et al.*, 2019). For the  
306 quantification of sesquiterpenes accumulation in pistils, 10 pistils per plant line were harvested at  
307 flower stage S9 and placed in 3 mL hexane. Camphor (3 nM) was added as internal standard (IS).  
308 Tissues were crushed in hexane with a potter, vortexed for 20 s, sonicated for 10 min at 40°C and

309 centrifuged at 2000 x *g* for 5 min. Supernatant was recovered, concentrated under nitrogen flow to  
310 c. 300 µL and analyzed by GC-MS (for more details see **Method S1**).

311 For the analysis of sesquiterpene emission from the inner surface of the *Petunia* tube, *Petunia*  
312 flowers at stage S9 were detached from their receptacle, their reproductive organs were carefully  
313 removed with forceps and flowers were placed in 5% sucrose solution. Emitted sesquiterpenes  
314 were collected by Stir Bar Sorptive Extraction (SBSE) by placing a magnetic Twister® (Gerstel,  
315 Germany) coated with Polydimethylsiloxane (PDMS) placed inside the upper part of the *Petunia*  
316 tube. After 48 h of collection, Twisters were eluted with 200 µL of hexane containing 2 nmol of  
317 IS, vortexed for 10 s and samples were analyzed by GC-MS (for more details see **Method S1**).

318

### 319 **Starch and Carotenoid measurements**

320 Tissues collected for the analysis are described in **Table S6**. The secreted nectar from WT  
321 ovaries was removed as much as possible using a tissue. WT and *eob2-3<sup>LofTAD</sup>* ovaries were cut  
322 just above the nectary glands. Limb and basal ovary samples were immediately flash-frozen in  
323 liquid nitrogen and stored at -80°C. Frozen samples were lyophilized using a Freeze Dry system  
324 (Lyoquest, from Swiss Vacuum technologies) for 4 days at -50°C, 10 mbar, in the dark.

325 Carotenoids were extracted from ~10 mg of freeze-dried nectaries and petals. Quantification of  
326 carotenoids was carried out with an HPLC system (UltiMate 3000, Thermo Scientific) (for more  
327 details see **Method S2**). Carbohydrates were extracted and quantified from a ~3 mg freeze-dried,  
328 ball-mill-ground, tissues with 1 mL of 80% ethanol for 20 min at 80 °C according to (Geest *et al.*,  
329 2016) with modifications (see **Method S3**).

330

### 331 **Detection of starch by Lugol staining**

332 Ovaries were placed in Lugol's solution (Carl Roth, N052) and a vacuum infiltration of 1 min was  
333 applied followed by a 10 min incubation. Samples were briefly rinsed with water before being  
334 photographed under a stereoscopic microscope (Nikon, SMZ1500) equipped with a camera (Leica,  
335 DMC6200). Flowers (w/o sepals) were cleared in 70% ethanol at 80 °C for 15 min, progressively  
336 rehydrated, stained with Lugol's solution (Carl Roth, N052) for 10 min and rinsed in water.

337 Pictures were taken before and after staining using a Canon EOS 60D camera and Canon 35 mm  
338 lens. For cellular resolution, images of the epidermal peel of petal limbs were captured with an  
339 optical microscope (Leica, DM2000 LED).

340



341 **Confocal microscopy, imaging of epidermal cells and cell size measurements**

342 Epidermal peels were taken from the outer rim area of the petal limb and placed on microscopy  
343 slides for confocal microscopy imaging. Epidermal peels of three flowers per line were taken for  
344 comparison. Images were taken with a laser scanning microscope 55 (Leica, SP5) using the  
345 differential interference contrast (DIC).

346

347 **Protein structure prediction**

348 The protein structures of EOB2 and eob2-2<sup>KO</sup> were predicted by AlphaFold (Jumper *et al.*, 2021).  
349 The structures were visualized and aligned by PyMOL (Version 2.5.3, Schrödinger LLC).

350

351 **Microsynteny analysis**

352 The microsynteny analysis was performed using GEvo tool from CoGe (Lyons *et al.*, 2008), with  
353 Peax4.03 genome for *P. axillaris* and ITAG release 2.4 genome for *S. lycopersicum*.

354

355 **Conserved cis-elements screening**

356 The promoter sequences of the selected genes were extracted (2kb upstream of the ATG) and  
357 scanned for EOB2 homolog-binding profile matrices (MA1408.1 and MA1037.1 defined in the  
358 JASPAR database), using FIMO v5.1.0 (Grant *et al.*, 2011). Identified motifs ( $P < 1e-4$ ) were  
359 counted <http://meme-suite.org/>.

360

361 **RESULTS**

362

363 **EOB1 and EOB2 are very similar in sequence and expression**

364 To determine the relationships between members of the SG19 R2R3-MYB family, we performed  
365 a phylogenetic analysis (**Fig. 1a**). SG19 members belonging to the Solanaceae were clearly  
366 separated from Arabidopsis. Nevertheless, protein alignments showed that the two main  
367 functional domains (RMD<sup>SG19</sup> and TAD) were highly conserved among the different species and  
368 among the different gene copies within species (**Figs 1b, S1**). Furthermore, microsynteny  
369 analysis established that *P. axillaris* *EOB1* and *EOB2* are the orthologs of *S. lycopersicum*  
370 *MYB24* and *MYB21*, respectively (**Fig. S2**).

371 Next, we performed a detailed analysis of the spatial and temporal expression of *P. axillaris*  
372 *EOB1* and *EOB2*. Different tissues and developmental stages of *P. axillaris* (**Figs 1c, S3** for  
373 definition of stages) were used to perform RT-qPCR of *EOB1* and *EOB2* (**Fig. 1d**). *EOB1* and  
374 *EOB2* expression was detected in the petal tube, petal limb, pistil, and a bit in the floral stem, but  
375 not in roots or leaves. Within the pistil, *EOB1* and *EOB2* were highly expressed in the basal  
376 ovary (BO) and the stigma, suggesting functions in nectary and stigma development (**Fig. 1d**).  
377 RT-qPCR on floral buds (without sepals) from S1 to S8 and on S10 open limbs from anthesis  
378 (D0) to 4 days after anthesis (D4) revealed that *EOB1* and *EOB2* started to be expressed from  
379 stage S3/S4, their expression increased over flower development and decreased 4 days after  
380 anthesis. However, RNA-sequencing data performed on basal ovaries at S5 and S10 and on petal  
381 limbs at S5, S7 and S10 (**Fig. 1e**) showed that *EOB1* expression is overall lower compared to that  
382 of *EOB2*. Moreover, while *EOB1* and *EOB2* are co-expressed in the flower, *EOB2* expression  
383 starts slightly before *EOB1*. Unlike previously thought, *EOB1* and *EOB2* functions are most  
384 likely not limited to regulation of the scent pathway and flower opening in *P. axillaris* (Spitzer-  
385 Rimon *et al.*, 2010; Colquhoun *et al.*, 2011; Spitzer-Rimon *et al.*, 2012).

386

### 387 **CRISPR-Cas9 as a tool to decipher R2R3-MYB SG19 complexity**

388 In order to obtain insight in the structure of the proteins, the proteins were characterized based on  
389 the literature. *EOB1* and *EOB2* genes encode for transcription factors of 202 and 197 amino acids  
390 (aa) respectively, that consist of an RMD<sup>SG19</sup> at the N-terminal and a TAD at the C-terminal part  
391 of the proteins (refer to the introduction for more details, **Fig. 2b**). The RMD<sup>SG19</sup> was previously  
392 shown to contain a nuclear localization signal (NLS). An *in silico* NLS mapper predictor  
393 ([https://nls-mapper.iab.keio.ac.jp/cgi-bin/NLS\\_Mapper\\_form.cgi](https://nls-mapper.iab.keio.ac.jp/cgi-bin/NLS_Mapper_form.cgi)) (Kosugi *et al.*, 2009) identified  
394 a putative bipartite NLS at the end of the RMD<sup>SG19</sup>  
395 (<sup>89</sup>RWSKIAKHLPGRTDNEIKNYWRTRIQKHIK<sup>118</sup>) in both *EOB1* and *EOB2* (**Fig. 2b Fig.**  
396 **S1**).

397 To elucidate the molecular and biological functions of *EOB1* and *EOB2* during *P. axillaris*  
398 flower development, targeted mutagenesis using CRISPR-Cas9 in *P. axillaris* P background was  
399 carried out (**Fig. 2a**). In total, one allele for *EOB1* and four alleles for *EOB2* were isolated by  
400 CRISPR-Cas9 (**Fig. 2b** and **Table S7**) and classified in different categories depending on their  
401 predicted protein conformations and putative molecular functions (**Fig. 2c**). The *eob1-1* allele  
402 showed a deletion of 31bp and is predicted to lead to nonfunctional product due to the truncated

403 RMD<sup>SG19</sup> and the absence of both the NLS and the TAD. The *eob2-1* mutant carried a deletion of  
404 364bp, which is also expected to cause a complete loss-of-function (**Figs 2b,c, S4a,b**). The *eob2-*  
405 2 allele presented a deletion of 7bp, this frameshift mutation resulted in an abnormal protein  
406 product. Alphafold2 was used to predict the 3D structure of EOB2 and *eob2-2* proteins (**Fig. 2d**).  
407 The RMD<sup>SG19</sup> domain was intact in *eob2-2*. In contrast, the C-terminal part of EOB2 was not  
408 conserved in *eob2-2*. This unrelated protein sequence may lead to destabilization of the *eob2-2*  
409 protein and disrupt RMD<sup>SG19</sup> DNA/protein binding capabilities. Even though the *eob2-1* and  
410 *eob2-2* encode quite different protein sequences, the two mutants displayed the same strong  
411 phenotype (see below). Therefore, most likely *eob2-1* and *eob2-2* both represent knockout alleles,  
412 referred as *eob2-1<sup>KO</sup>* and *eob2-2<sup>KO</sup>*. The *eob2-3* and *eob2-4* alleles contained deletions of 5bp or  
413 2bp, respectively. These mutations removed the transcriptional activation domain (TAD) but  
414 retained an intact RMD<sup>SG19</sup> (**Fig. 2b,c**). The *eob2-3* and *eob2-4* truncated proteins retain the  
415 nuclear localization signal, bind DNA, and can interact with protein partners but lack their  
416 transactivation activity. Thus, *eob2-3* and *eob2-4* are referred to as loss-of-TAD alleles (*eob2-*  
417 *3<sup>LofTAD</sup>* and *eob2-4<sup>LofTAD</sup>*).

418

### 419 **EOB2 is a regulator of EOB1**

420 The knockout mutants in *EOB1* and *EOB2* caused very different phenotypes. No visible  
421 developmental phenotypes were observed in *eob1-1<sup>KO</sup>* (**Figs 2e,f, 3a**), but the emission of the  
422 major scent compounds was reduced compared to the wild type (**Fig. 3b**) as previously observed  
423 in *Petunia hybrida* *EOB1-RNAi* lines (Spitzer-Rimon *et al.*, 2012). Moreover, *IGS* expression  
424 was induced in *Petunia* leaves after *EOB1* transient expression (**Fig. 3e**). We conclude that *EOB1*  
425 is essential for floral volatile benzenoid/phenylpropanoid (FVBP) production, even in the  
426 presence of active *EOB2*.

427 The flowers of the *eob2* knockout alleles, *eob2-1<sup>KO</sup>* and *eob2-2<sup>KO</sup>*, failed to enter anthesis and  
428 prematurely senesced as closed buds. Flower initiation was not affected but flower bud growth  
429 was delayed after reaching ~2 cm (stage S4) and the buds prematurely entered senescence at ~3.5  
430 cm (S5) (**Figs 2e,f, 3a, S5**). After reaching S5, the flower bud stopped growing and gradually  
431 senesced: the petal limb tip started to soften, the flower bud turned yellow/brown and the flower  
432 bud was completely brown/dead. At 16 weeks after germination, the difference between mutant  
433 plants and wild-type was remarkable: 100% of fully opened flowers in the wild-type against 0%  
434 in the mutant lines (**Fig. 3a**). As the heterozygotes are phenotypically wild type, we conclude that

435 the *eob2-1<sup>KO</sup>* and *eob2-2<sup>KO</sup>* alleles are recessive (**Fig. S6**). The fact that expression of *EOB2*  
436 precedes *EOB1* expression (**Fig. 1e**) suggests that *EOB2* may be an activator of *EOB1*. Indeed,  
437 *EOB2* expression is independent of *EOB1* (**Fig. 3c,e**) while *EOB1* expression is activated by  
438 *EOB2* (**Fig. 3d,e**), probably by binding to the defined “SG19 MYB-binding site” in the *EOB1*  
439 promoter (**Figs 3f, S7a**). Moreover, no additional effects were observed when comparing the  
440 *eob2-2<sup>KO</sup>* single mutant to the *eob1-1<sup>KO</sup>/eob2-2<sup>KO</sup>* double mutant flowers (**Figs 3a, S9**).  
441 Therefore, *EOB1* is downstream of *EOB2*.

442

### 443 **The loss-of-TAD mutants display floral organ maturation defects**

444 The *eob2* knockout alleles described so far displayed early senescence and did not reach anthesis,  
445 which makes it impossible to investigate *EOB2* function(s) beyond stage 5. Based on its  
446 expression pattern (**Fig. 1d**), *EOB2* may also function in later floral developmental stages. The  
447 loss-of-TAD (LofTAD) mutants, *eob2-3<sup>LofTAD</sup>* and *eob2-4<sup>LofTAD</sup>*, allowed us to study *EOB2*  
448 function at the later developmental stages.

449 The *eob2-3<sup>LofTAD</sup>* and *eob2-4<sup>LofTAD</sup>* homozygous single mutants caused identical pleiotropic floral  
450 phenotypes with floral organ maturation defects and juvenile characteristics at late stages (**Fig.**  
451 **2f**). The *eob2-3<sup>LofTAD</sup>* mutant was used for further analysis. Compared to the wild type, petal tubes  
452 were shorter, petals did not fully open, limbs were smaller and had greener petal veins (**Fig. 4a,f**).  
453 Both wild-type and LofTAD limbs were UV-absorbing (**Fig. S8**). Concerning the reproductive  
454 organs, no stamen/pollen phenotypes were observed. In contrast, we noticed phenotypes in style,  
455 stigma, and nectary. Styles were twisted, which can be interpreted as an indirect phenotype due to  
456 the mechanical constraints applied by the reduced petal growth (**Fig. 4b**).

457 While droplets of exudate were present on wild-type stigmas, the mutant had dry stigma surfaces.  
458 A key function of the stigma exudate is pollen hydration, a prerequisite for pollen tube elongation  
459 and fertilization. Indeed, *eob2-3<sup>LofTAD</sup>* failed to hydrate pollen, impairing seed set. Seed yield was  
460 increased when the dry *eob2-3<sup>LofTAD</sup>* stigmas were treated with wild-type stigma exudate (**Fig.**  
461 **4c**). Ovule number and development were not impacted (**Fig. 4d**). After pollination and  
462 fertilization, the style was detached from the fruit in the wild type but not in the mutants (**Fig.**  
463 **4c,e**). Nectar secretion was disrupted (**Fig. 4g**) and carotene levels were reduced (**Fig. 4h**)  
464 indicating defective nectary maturation.

465 Several SG19 members have been shown to play a role in the production of diverse floral  
466 volatiles in a range of species (see introduction). In the *eob2-3<sup>LofTAD</sup>* petal limbs, benzaldehyde

467 and methylbenzoate were absent, in line with a decreased expression of *ODO1* and *EOB1* (**Fig.**  
468 **4i,j**). The emission of terpene volatiles from the floral tube was reduced, as well as their  
469 accumulation in the stigma (**Fig. 4k,l**). In *P. hybrida*, *TPS1* was shown to regulate terpene  
470 volatile synthesis and emission from the tube (Boachon *et al.*, 2019). In *eob2-3<sup>LofTAD</sup>* petal tube,  
471 *TPS1* expression was also reduced (**Fig. 4m**).  
472 Next, we analyzed the F1 progenies. The *eob2-3<sup>LofTAD</sup>/+* and *eob2-4<sup>LofTAD</sup>/+* heterozygous flowers  
473 displayed an intermediate phenotype (intermediate flower angle opening, nectar volume and  
474 methylbenzoate level) indicating that *LofTAD* alleles are semi-dominant (**Fig. S6**). This  
475 intermediate phenotype is compatible with a competition between the products of the wild-type  
476 and the *LofTAD* mutants for the same DNA-cis-elements.

477

#### 478 **EOB2 prevents flower senescence during flower development by inhibiting ethylene** 479 **synthesis**

480 The contrasting phenotypes of *eob2* knockout vs *LofTAD* might be explained by differences at  
481 the transcriptional level. Therefore, a transcriptome analysis of S5 petal limb from WT, *eob2-1<sup>KO</sup>*  
482 and *eob2-3<sup>LofTAD</sup>* was carried out (**Fig. 5a**). *EOB2* expression was significantly downregulated in  
483 the knockout line while no significant expression differences were observed in the wild-type vs  
484 *LofTAD* comparison (**Fig. S4c**). This reinforces the notion that *eob2-1<sup>KO</sup>* is a complete knockout,  
485 while *eob2-3<sup>LofTAD</sup>* retains partial activity. Whereas 23% of the genes were differentially regulated  
486 in the knockout (*eob2-1<sup>KO</sup>*), only 4.5% were differentially expressed in the *LofTAD* (*eob2-*  
487 *3<sup>LofTAD</sup>*). Again, this is in line with partial activity of *eob2-3<sup>LofTAD</sup>*. Most of the 4.5% were  
488 regulated in the same direction (either up- or down-regulated) in the two genotypes, supporting  
489 that both alleles partly act on the same pathways. Interestingly, in both mutant backgrounds, the  
490 majority of the DEGs was up-regulated. As structural data strongly indicate that *EOB2* is a  
491 transcriptional activator (see introduction), the observed upregulation must be an indirect effect  
492 (indirect targets and/or mediated by interacting factors). Moreover, an *in silico* scanning promoter  
493 analysis revealed that the down-regulated gene promoters displayed a significant enrichment of  
494 the SG19 binding site matrices, while it was not the case for the up-regulated gene promoters  
495 (**Table S8** and **Fig. S11**).

496 Within the large proportion of *eob2-1<sup>KO</sup>*-specific DEGs, GO terms associated with senescence  
497 were over-represented (**Fig. 5b**). Among them, several *ACS* and *ACO* genes encoding enzymes  
498 responsible for ethylene synthesis were up-regulated (**Fig. 5c** and **Table S9**) as well as many

499 ethylene response factors (ERF) and senescence-associated genes (SAG). Genes related to  
500 cellular processes maintenance (translation, cellular trafficking, mitotic cell cycle, etc.) were  
501 down-regulated, presumably as a consequence of senescence.  
502 Ethylene is a key hormone promoting flower senescence and blocking ethylene sensitivity  
503 partially restored the RNAi-*EOB2* flower phenotypes in *P. hybrida* and *N. attenuata* (Colquhoun  
504 *et al.*, 2011). To obtain direct proof that ethylene production is activated prematurely in *eob2-1<sup>KO</sup>*  
505 and *eob2-2<sup>KO</sup>* compared to wild-type flowers, we quantified ethylene emission from S5 flower  
506 buds before the first signs of senescence. Ethylene levels in *eob2-1<sup>KO</sup>* flower buds at S5 were  
507 higher compared to wild-type (**Fig. 5d**). Since *EOB2* is expressed in both petal and pistil (**Fig.**  
508 **1c**), ethylene measurements were performed on dissected petal and pistil from S5 flower buds.  
509 We noticed a strong contribution from both floral organs in releasing ethylene. In parallel, a 1-  
510 MCP treatment (ethylene action inhibitor) was continuously applied on wild-type, *eob2-1<sup>KO</sup>* and  
511 *eob2-3<sup>LofTAD</sup>* plants. 1-MCP treatment caused a partial rescue of the *eob2-1<sup>KO</sup>* flower senescence  
512 phenotype but negligible floral developmental effects on wild-type and *eob2-3<sup>LofTAD</sup>* (**Figs 5e, S9,**  
513 **S10**). Similar results were obtained with the other allele *eob2-2<sup>KO</sup>*. Though *eob2-1<sup>KO</sup>* or *eob2-2<sup>KO</sup>*  
514 flowers reached anthesis after 1-MCP treatment, they did not fully open, were scentless and  
515 morphologically similar to *eob2-3<sup>LofTAD</sup>* or *eob2-4<sup>LofTAD</sup>* flowers.

516

### 517 **EOB2 activates pathways of secondary metabolism**

518 We took advantage of the powerful *eob2-3<sup>LofTAD</sup>* mutant to (1) identify *EOB2* transcriptional  
519 targets and (2) unravel to what extent nectary and petal limb maturation are regulated by the same  
520 genetic pathway. To do so, we compared the transcriptomes of wild-type and *eob2-3<sup>LofTAD</sup>* petal  
521 limb and nectary, at S5 and S10 (**Fig. 6a**). The analysis of the differentially expressed genes  
522 (DEGs) revealed a higher proportion of up-regulated genes in each condition and the number of  
523 DEGs was higher at S10 than S5 in both floral organs (**Fig. 6a**). Since *EOB2* is thought to be a  
524 transcriptional activator (see introduction), the down-regulated genes are potential direct targets.  
525 Among the down-regulated genes, a significant enrichment of promoters presented SG19 binding  
526 sites, which was not the case for the up-regulated genes (**Figs 6b, S11 and Table S8**). Sixty genes  
527 were commonly down-regulated in the four different conditions (**Fig. 6c**). Among them, we  
528 found seven genes encoding enzymes of the shikimate/phenylpropanoid and four carotenoid  
529 biosynthetic genes (**Fig. 6d**). These genes are likely to be direct targets of *EOB2* and to support  
530 this founding some homologs were also identified as direct targets in other species (**Table S2**).

531 Indeed, SG19 binding sites were identified at least once in each of the 11 promoters tested, while  
532 only five promoters presented the exact motif characteristic for SG19 (**Fig. 6d**). This data  
533 provides evidence that EOB2 is a direct activator candidate of genes involved in shikimate,  
534 phenylpropanoid and carotenoid maturation pathways in both limb and nectary tissues (**Fig. S12**).

535

### 536 **Carbohydrate metabolism is involved in floral organ maturation**

537 Nectary and limb are mostly sink tissues, dependent on the surrounding photosynthetic tissues to  
538 provide carbohydrates for their active growth. Starch that is stored at early stages is mobilized  
539 later to support respiration, growth and maturation (Streb & Zeeman, 2012). A GO-term  
540 enrichment analysis was performed on the down-regulated genes from the four conditions. Only  
541 two GO-terms were significantly co-enriched in the four conditions: ‘TCA cycle’ and ‘glycolytic  
542 process’, meaning that high energy carbohydrate breakdown was impaired in both *eob2-3<sup>LofTAD</sup>*  
543 nectary and limb (**Fig. 7a**). We also evaluated whether other components of carbohydrate  
544 metabolism were impacted. One gene encoding a beta-amylase (*BAM*) was strongly down-  
545 regulated in both *eob2-3<sup>LofTAD</sup>* floral organs compared to wild-type (**Fig. 7b**), suggesting that  
546 starch degradation was also impaired (**Fig. 7c**).

547 We next evaluated starch levels in wild-type vs *eob2-3<sup>LofTAD</sup>* in both petals and nectaries using  
548 IKI staining. During wild-type flower development, we observed an accumulation of large  
549 amounts of starch at stage S5 and decreased levels at stage 10, while starch levels remained high  
550 in *eob2-3<sup>LofTAD</sup>* (**Fig. 7d,e**). In nectary at S10, starch was only detected within the wild-type  
551 stomata, whereas *eob2-3<sup>LofTAD</sup>* nectary stained heavily for starch, comparable to S5 immature  
552 nectary (**Fig. 7d**). Full petal and petal limb epidermal peels, also revealed that *eob2-3<sup>LofTAD</sup>*  
553 retained more starch granules compared to wild-type (**Fig. 7e,f**). In addition, *eob2-3<sup>LofTAD</sup>* petal  
554 limb epidermal cells were smaller. The Lugol results were confirmed by starch content  
555 quantification (**Fig. 7g**). These results indicated that the carbohydrate breakdown was reduced in  
556 both nectary and limb of the *eob2-3<sup>LofTAD</sup>* mutant (**Fig. 7c**). This is consistent with the juvenile  
557 character of the *eob2-3<sup>LofTAD</sup>* mutant.

558

## 559 **DISCUSSION**

560

561 **Different promoter sequences and subtle differences in protein coding sequences drive the**  
562 **functional divergence of *EOB1* and *EOB2***

563 The *EOB1* and *EOB2* genes encode closely related members of subgroup 19 R2R3-MYB  
564 transcription factors. Nevertheless, *eob1* and *eob2* mutants display radically different phenotypes.  
565 Loss-of-function of *EOB1* causes a decrease in scent emission, whereas *EOB2* is extremely  
566 pleiotropic. Thus, there must be subtle differences in protein sequence and/or expression that are  
567 responsible for these highly distinct phenotypes. *EOB2* is expressed slightly earlier than *EOB1*,  
568 *EOB2* induces *EOB1* expression and a potential *EOB2*-binding site is present in the *EOB1*  
569 promoter, potentially explaining their extremely similar expression patterns. Phylogenetic and  
570 microsynteny analysis reveal that species with a single SG19 member, the gene is closer to the  
571 petunia *EOB2* than to *EOB1*. It might be that *EOB2* ancestor evolved as a driver of flower  
572 maturation, while petunia *EOB1* appeared later during evolution from *EOB2* duplication and  
573 gained a specific function in scent production (scent booster), notably due to its divergent  
574 promoter (**Fig. S7**) and the associated delayed expression pattern compared to *EOB2*, with a peak  
575 at anthesis.

576 As *EOB1* expression was strongly reduced in an *eob2<sup>KO</sup>* background, while *eob1<sup>KO</sup>* mutants had  
577 normal *EOB2* expression, *EOB2* must be a major activator of *EOB1*. In parallel, a previous study  
578 revealed that PhERF6 interacts with *EOB1* to regulate scent biosynthesis, but not with *EOB2*  
579 (Liu *et al.*, 2017). Promoter differences as well as subtle differences in protein-protein  
580 interactions underlie the loss of scent phenotype in the *eob1<sup>KO</sup>* mutant.

581  
582 **Nectary and limb are sink tissues, that rely on common pathways for their maturation**  
583 At later developmental stages, the LofTAD mutant flowers retained starch, did not produce  
584 benzenoid/phenylpropanoid volatiles, produced less terpenoids and presented a smaller, greener,  
585 not fully opened corolla (**Figs 4,7**). In line with this, transcriptomic data revealed that genes  
586 encoding enzymes of both primary and secondary metabolisms were decreased in immature  
587 tissues compared to those of the WT. We consider following options: it could be that both  
588 primary and secondary metabolisms are dependent on *EOB2* or that *EOB2* directly regulates only  
589 one of these two processes and that the other process is reduced as a consequence. The presence  
590 of *EOB2*-binding sites in promoters of genes in the shikimate/phenylpropanoid and carotenoid  
591 pathways would support the second option. In that case, the decrease of energy-demanding  
592 secondary metabolites production could reduce carbohydrate flux through feedback inhibition.

593  
594 **Comparisons with the R2R3-MYB SG19 functions previously reported in the literature**



595 In the introduction, we asked the question whether the conflicting data on the functions of SG19  
596 R2R3-MYBs reported within and between different species were due to species specificity, to the  
597 methods used, to the focus of the study on a particular organ or to the multi-functionality of the  
598 SG19 R2R3-MYBs. Here, we used well-defined mutants and revealed in a single system the  
599 complexity of the SG19 R2R3-MYB functions.

600 Comparable to *eob2* KO, premature flower senescence has been described for strong RNAi lines  
601 targeting *EOB2* homologs in *P. hybrida* and *N. attenuata* (Colquhoun *et al.*, 2011). By contrast  
602 and similar to *eob2* LofTAD, immature floral organ phenotypes were reported in other tobacco  
603 RNAi lines targeting *MYB305* (Liu *et al.*, 2009; Liu & Thornburg, 2012). We can speculate that  
604 those RNAi lines had an increased proportion of alternative splicing variants with an intact  
605 R2R3-MYB and no TAD (RNAi targeted the C-ter) or that the silencing was incomplete making  
606 it possible to block the senescence but not enough to induce transcription. The VIGS performed  
607 in *P. hybrida* targeting *EOB2* only revealed scent related phenotypes, so it could be that the  
608 silencing was incomplete or that *EOB1* instead of *EOB2* was targeted in this study.

609 The expression pattern of tobacco MYB305 (Liu *et al.*, 2009) was similar to *Petunia* *EOB2*,  
610 while expression of Arabidopsis *AtMYB21* and *AtMYB24* was also detected in stamens and these  
611 proteins play a major role in Arabidopsis anther maturation (Qi *et al.*, 2015). Out of those  
612 different expression patterns and functions, we concluded that in Arabidopsis SG19 R2R3-MYB  
613 members were recruited for stamen maturation while other factors were selected in pollinator-  
614 dependent species such as *Petunia* or *Nicotiana*. Except for the stamens, Arabidopsis and *Petunia*  
615 SG19 genes have similar spatial expression patterns and share functions (nectary maturation,  
616 flower opening), however other functions are specific for *Petunia* (senescence, FVBP) or for  
617 Arabidopsis (flavonols) (Zhang *et al.*, 2021b). In addition to the differences in floral organ  
618 expression, it appears that during evolution, different partners and target genes were recruited by  
619 the SG19 R2R3-MYBs (**Tables S1, S2**).

620

### 621 **One gene, two mutations, contrasting phenotypes**

622 The *eob2*<sup>KO</sup> mutations display premature flower senescence, whereas the semi-dominant  
623 *eob2*<sup>LofTAD</sup> alleles retain the RMD<sup>SG19</sup> functions specifically and *eob2*<sup>LofTAD</sup> mutants and show  
624 multiple flower maturation defects resulting in juvenile flowers (**Fig. 8**). The conclusions are the  
625 following: (1) *EOB2* is a multifunctional protein, (2) *EOB2* transcriptional activity drives flower  
626 maturation and (3) the R2R3-MYB domain is, in addition to its DNA-binding role in

627 transcription, involved in the regulation of indirect senescence-related targets through an  
628 unknown mechanism. Cases of nonfunctional versus partially functional gene product showing  
629 different phenotypes are rare in the literature, an example is the tomato MADS-box gene *RIN* (for  
630 *ripening inhibitor*) where the *rin-knockout* (Ito *et al.*, 2017) and semi-dominant *rinG2* (Ito *et al.*,  
631 2021) alleles were leading to different tomato fruit phenotypes. Proper conclusions about the  
632 function(s) of the protein require a careful analysis of the protein structure before targeting a TF  
633 gene by mutagenesis.

634

### 635 **Complexity of SG19 MYB factors protein functions**

636 The genetic processes that underlie the initiation and determination of the floral organs have been  
637 well studied in *Arabidopsis*, snapdragon and *Petunia* (Coen & Meyerowitz, 1991;  
638 Vandebussche *et al.*, 2004; Morel *et al.*, 2018), and are quite well conserved between species  
639 (Soltis *et al.*, 2007). Floral diversity mainly arises during subsequent maturation and serves to  
640 adapt flowers to specific guilds of pollinators (Schiestl & Johnson, 2013). This aspect may be  
641 negligible in a selfing species such as *Arabidopsis thaliana* but is essential in animal-pollinated  
642 species. The versatility of SG19 MYB factors and their many interacting regulatory factors  
643 appear to be well suited to adapt flowers for optimal pollination. SG19 MYB factors affect  
644 multiple aspects of flower maturation, with potential impact on the functions of the flower. These  
645 include floral morphology (Yarahmadov *et al.*, 2020), scent (Spitzer-Rimon *et al.*, 2010), nectar  
646 (Liu *et al.*, 2009, p. 305; Liu & Thornburg, 2012) and color (Wang *et al.*, 2022), but also plant  
647 defense against microorganisms mediated by the antimicrobial activity of terpenes (Boachon *et*  
648 *al.*, 2019) or compounds present in the stigma exudate/nectar (Kurilla *et al.*, 2019).

649 While part of the confusion about the roles of SG19 MYB factors in flower development may be  
650 due to the use of different techniques, it is also clear that data on EOB2 and its homologs cannot  
651 be extrapolated from one species to the next, possibly reflecting the diversity of plant-pollinator  
652 interactions.

653

654

### 655 **ACKNOWLEDGEMENTS**

656 This work was supported by grants from the Swiss National Science Foundation  
657 (31003A\_182340) and the European Union (ERC-ADG 741354). We would like to thank the  
658 Next Generation Sequencing Platform of the University of Bern for performing the high-

659 throughput sequencing experiments and the Interfaculty Bioinformatics Unit of the University of  
660 Bern for providing computational infrastructure and support with bioinformatic analyses. We  
661 thank Christopher Ball, Jasmin Sekulovski, and Sarah Dolder for taking care of our *Petunia*  
662 plants. We are grateful to Patrick Ryan and Ying Li for providing their GO annotations, Diane  
663 Bonnet for advice on microscopy, Aya Assamene for technical support, and Chaobin Li for  
664 bioinformatics supports as well as helpful discussion and proof-reading.

665

#### 666 **AUTHOR CONTRIBUTIONS**

667 M.C. and C.K. conceived and designed the experiments. M.C. generated the CRISPR-Cas9 lines,  
668 performed the phenotyping/pictures, the 1-MCP treatments, the starch staining using Lugol, the  
669 RT-qPCR with the technical support of L.J.. G.C. performed the protein structures prediction  
670 with AlphaFold. R.Halitschke performed the ethylene measurements. B.B. and D.P.B. performed  
671 the terpene measurements. R.Heutink and J.V. performed the starch and carotenoid  
672 measurements. M.C., M.B. and G.G. performed the RNA-seq analysis. M.C. and C.K. wrote the  
673 article.

674

#### 675 **DATA AVAILABILITY**

676 Raw reads are available on NCBI Sequence Read Archive (SRA), under the BioProject accession  
677 PRJNA797226 (reviewer link:  
678 <https://dataview.ncbi.nlm.nih.gov/object/PRJNA797226?reviewer=pa7i8vmprfq16vvu67ui6tqvui>)  
679 . Plasmids and seeds produced in this study are available from C.K. on request.

680

#### 681 **COMPETING INTERESTS**

682 None declared.

683

#### 684 **REFERENCES**

685

686 **Amrad A, Moser M, Mandel T, de Vries M, Schuurink RC, Freitas L, Kuhlemeier C. 2016.**  
687 **Gain and Loss of Floral Scent Production through Changes in Structural Genes during Pollinator-**  
688 **Mediated Speciation. *Current biology: CB* 26: 3303–3312.**

689 **Andrews S. 2022.** Babraham Bioinformatics - FastQC A Quality Control tool for High  
690 Throughput Sequence Data.

691 **Battat M, Eitan A, Rogachev I, Hanhineva K, Fernie A, Tohge T, Beekwilder J, Aharoni A.**  
692 **2019.** A MYB Triad Controls Primary and Phenylpropanoid Metabolites for Pollen Coat  
693 Patterning. *Plant Physiology* **180**: 87–108.

694 **Bian S, Sui X, Wang J, Tian T, Wang C, Zhao X, Liu X, Fang N, Zhang Y, Liu Y, et al.**  
695 **2021.** NtMYB305a binds to the jasmonate-responsive GAG region of NtPMT1a promoter to  
696 regulate nicotine biosynthesis. *Plant Physiology*.

697 **Boachon B, Lynch J, Ray S, Yuan J, Caldo K, Junker R, Kessler S, Morgan J, Dudareva N.**  
698 **2019.** Natural fumigation as a mechanism for volatile transport between flower organs. *Nature*  
699 *Chemical Biology* **15**: 583–588.

700 **Brandenburg A, Kuhlemeier C, Bshary R. 2012.** Hawkmoth Pollinators Decrease Seed Set of  
701 a Low-Nectar *Petunia axillaris* Line through Reduced Probing Time. *Current Biology* **22**: 1635–  
702 1639.

703 **Cheng H, Song S, Xiao L, Soo HM, Cheng Z, Xie D, Peng J. 2009.** Gibberellin Acts through  
704 Jasmonate to Control the Expression of MYB21, MYB24, and MYB57 to Promote Stamen  
705 Filament Growth in *Arabidopsis*. *PLOS Genetics* **5**: e1000440.

706 **Chopy M, Morel P, Rodrigues Bento S, Vandenbussche M. 2020.** Genome editing by  
707 CRISPR-Cas9 technology in *Petunia hybrida*. *Acta Horticulturae*: 209–218.

708 **Coen ES, Meyerowitz EM. 1991.** The war of the whorls: genetic interactions controlling flower  
709 development. *Nature* **353**: 31–37.

710 **Colquhoun TA, Schwieterman ML, Wedde AE, Schimmel BCJ, Marciniak DM, Verdonk**  
711 **JC, Kim JY, Oh Y, Gális I, Baldwin IT, et al. 2011.** EOBII Controls Flower Opening by  
712 Functioning as a General Transcriptomic Switch. *Plant Physiology* **156**: 974–984.

713 **Edgar RC. 2004.** MUSCLE: multiple sequence alignment with high accuracy and high  
714 throughput. *Nucleic Acids Research* **32**: 1792–1797.

715 **Edwards K, Johnstone C, Thompson C. 1991.** A simple and rapid method for the preparation  
716 of plant genomic DNA for PCR analysis. *Nucleic Acids Research* **19**: 1349.

717 **Geest G van, Choi YH, Arens P, Post A, Liu Y, Meeteren U van. 2016.** Genotypic differences  
718 in metabolomic changes during storage induced-degreening of chrysanthemum disk florets.  
719 *Postharvest Biology and Technology* **115**: 48–59.

720 **Grant CE, Bailey TL, Noble WS. 2011.** FIMO: scanning for occurrences of a given motif.  
721 *Bioinformatics* **27**: 1017–1018.

722 **Guindon S, Dufayard J-F, Lefort V, Anisimova M, Hordijk W, Gascuel O. 2010.** New  
723 Algorithms and Methods to Estimate Maximum-Likelihood Phylogenies: Assessing the  
724 Performance of PhyML 3.0. *Systematic Biology* **59**: 307–321.

- 725 **Hoballah ME, Stuurman J, Turlings TCJ, Guerin PM, Connétable S, Kuhlemeier C. 2005.**  
726 The composition and timing of flower odour emission by wild *Petunia axillaris* coincide with the  
727 antennal perception and nocturnal activity of the pollinator *Manduca sexta*. *Planta* **222**: 141–150.
- 728 **Huang H, Gao H, Liu B, Qi T, Tong J, Xiao L, Xie D, Song S. 2017.** Arabidopsis MYB24  
729 Regulates Jasmonate-Mediated Stamen Development. *Frontiers in Plant Science* **8**.
- 730 **Huang H, Gong Y, Liu B, Wu D, Zhang M, Xie D, Song S. 2020.** The DELLA proteins  
731 interact with MYB21 and MYB24 to regulate filament elongation in Arabidopsis. *BMC Plant*  
732 *Biology* **20**: 64.
- 733 **Ito Y, Nakamura N, Kotake-Nara E. 2021.** Semi-dominant effects of a novel ripening inhibitor  
734 (*rin*) locus allele on tomato fruit ripening. *PLOS ONE* **16**: e0249575.
- 735 **Ito Y, Nishizawa-Yokoi A, Endo M, Mikami M, Shima Y, Nakamura N, Kotake-Nara E,**  
736 **Kawasaki S, Toki S. 2017.** Re-evaluation of the *rin* mutation and the role of RIN in the  
737 induction of tomato ripening. *Nature Plants* **3**: 866–874.
- 738 **Jumper J, Evans R, Pritzel A, Green T, Figurnov M, Ronneberger O, Tunyasuvunakool K,**  
739 **Bates R, Žídek A, Potapenko A, et al. 2021.** Highly accurate protein structure prediction with  
740 AlphaFold. *Nature* **596**: 583–589.
- 741 **Ke Y, Abbas F, Zhou Y, Yu R, Fan Y. 2021.** Auxin-Responsive R2R3-MYB Transcription  
742 Factors HcMYB1 and HcMYB2 Activate Volatile Biosynthesis in *Hedychium coronarium*  
743 Flowers. *Frontiers in Plant Science* **0**.
- 744 **Kim D, Langmead B, Salzberg SL. 2015.** HISAT: a fast spliced aligner with low memory  
745 requirements. *Nature Methods* **12**: 357–360.
- 746 **Kosugi S, Hasebe M, Tomita M, Yanagawa H. 2009.** Systematic identification of cell cycle-  
747 dependent yeast nucleocytoplasmic shuttling proteins by prediction of composite motifs.  
748 *Proceedings of the National Academy of Sciences of the United States of America* **106**: 10171–  
749 10176.
- 750 **Kurilla A, Toth T, Dorgai L, Darula Z, Lakatos T, Silhavy D, Kerenyi Z, Dallmann G.**  
751 **2019.** Nectar- and stigma exudate-specific expression of an acidic chitinase could partially  
752 protect certain apple cultivars against fire blight disease. *Planta* **251**: 20.
- 753 **Liao Y, Smyth GK, Shi W. 2014.** featureCounts: an efficient general purpose program for  
754 assigning sequence reads to genomic features. *Bioinformatics* **30**: 923–930.
- 755 **Liu G, Ren G, Guirgis A, Thornburg RW. 2009.** The MYB305 Transcription Factor Regulates  
756 Expression of Nectarin Genes in the Ornamental Tobacco Floral Nectary. *The Plant Cell* **21**:  
757 2672–2687.
- 758 **Liu G, Thornburg RW. 2012.** Knockdown of MYB305 disrupts nectary starch metabolism and  
759 floral nectar production. *The Plant Journal* **70**: 377–388.

760 **Liu F, Xiao Z, Yang L, Chen Q, Shao L, Liu J, Yu Y. 2017.** PhERF6, interacting with EOBI,  
761 negatively regulates fragrance biosynthesis in petunia flowers. *New Phytologist* **215**: 1490–1502.

762 **Love MI, Huber W, Anders S. 2014.** Moderated estimation of fold change and dispersion for  
763 RNA-seq data with DESeq2. *Genome Biology* **15**: 550.

764 **Lyons E, Pedersen B, Kane J, Alam M, Ming R, Tang H, Wang X, Bowers J, Paterson A,**  
765 **Lisch D, et al. 2008.** Finding and Comparing Syntenic Regions among Arabidopsis and the  
766 Outgroups Papaya, Poplar, and Grape: CoGe with Rosids. *Plant Physiology* **148**: 1772–1781.

767 **Ma D, Constabel CP. 2019.** MYB Repressors as Regulators of Phenylpropanoid Metabolism in  
768 Plants. *Trends in Plant Science* **24**: 275–289.

769 **Mallona I, Lischewski S, Weiss J, Hause B, Egea-Cortines M. 2010.** Validation of reference  
770 genes for quantitative real-time PCR during leaf and flower development in *Petunia hybrida*.  
771 *BMC Plant Biology* **10**: 4.

772 **Mandaokar A, Thines B, Shin B, Lange BM, Choi G, Koo YJ, Yoo YJ, Choi YD, Choi G,**  
773 **Browse J. 2006.** Transcriptional regulators of stamen development in Arabidopsis identified by  
774 transcriptional profiling. *The Plant Journal* **46**: 984–1008.

775 **Martin M. 2011.** Cutadapt removes adapter sequences from high-throughput sequencing reads.  
776 *EMBnet.journal* **17**: 10–12.

777 **Medina-Puche L, Molina-Hidalgo FJ, Boersma M, Schuurink RC, López-Vidriero I, Solano**  
778 **R, Franco-Zorrilla J-M, Caballero JL, Blanco-Portales R, Muñoz-Blanco J. 2015.** An R2R3-  
779 MYB Transcription Factor Regulates Eugenol Production in Ripe Strawberry Fruit Receptacles.  
780 *Plant Physiology* **168**: 598–614.

781 **Moerkercke AV, Haring MA, Schuurink RC. 2011.** The transcription factor EMISSION OF  
782 BENZENOIDES II activates the MYB ODORANT1 promoter at a MYB binding site specific for  
783 fragrant petunias. *The Plant Journal* **67**: 917–928.

784 **Morel P, Heijmans K, Ament K, Chopy M, Trehin C, Chambrier P, Bento SR, Bimbo A,**  
785 **Vandenbussche M. 2018.** The Floral C-Lineage Genes Trigger Nectary Development in *Petunia*  
786 and Arabidopsis. *The Plant Cell* **30**: 2020–2037.

787 **Moyano E, Martínez-García JF, Martín C. 1996.** Apparent redundancy in myb gene function  
788 provides gearing for the control of flavonoid biosynthesis in antirrhinum flowers. *The Plant Cell*  
789 **8**: 1519–1532.

790 **NAKAGAWA T, SUZUKI T, MURATA S, NAKAMURA S, HINO T, MAEO K, TABATA**  
791 **R, KAWAI T, TANAKA K, NIWA Y, et al. 2007.** Improved Gateway Binary Vectors: High-  
792 Performance Vectors for Creation of Fusion Constructs in Transgenic Analysis of Plants.  
793 *Bioscience, Biotechnology, and Biochemistry* **71**: 2095–2100.

794 **Niwa T, Suzuki T, Takebayashi Y, Ishiguro R, Higashiyama T, Sakakibara H, Ishiguro S.**  
795 **2018.** Jasmonic acid facilitates flower opening and floral organ development through the

796 upregulated expression of SIMYB21 transcription factor in tomato. *Bioscience, Biotechnology,*  
797 *and Biochemistry* **82**: 292–303.

798 **Okonechnikov K, Golosova O, Fursov M, the UGENE team. 2012.** Unipro UGENE: a unified  
799 bioinformatics toolkit. *Bioinformatics* **28**: 1166–1167.

800 **Patrick RM, Huang X-Q, Dudareva N, Li Y. 2021.** Dynamic histone acetylation in floral  
801 volatile synthesis and emission in petunia flowers. *Journal of Experimental Botany* **72**: 3704–  
802 3722.

803 **Qi T, Huang H, Song S, Xie D. 2015.** Regulation of Jasmonate-Mediated Stamen Development  
804 and Seed Production by a bHLH-MYB Complex in Arabidopsis. *The Plant Cell* **27**: 1620–1633.

805 **Reeves PH, Ellis CM, Ploense SE, Wu M-F, Yadav V, Tholl D, Chételat A, Haupt I,**  
806 **Kennerley BJ, Hodgens C, et al. 2012.** A Regulatory Network for Coordinated Flower  
807 Maturation. *PLOS Genetics* **8**: e1002506.

808 **Sablowski R w., Moyano E, Culianez-Macia F a., Schuch W, Martin C, Bevan M. 1994.** A  
809 flower-specific Myb protein activates transcription of phenylpropanoid biosynthetic genes. *The*  
810 *EMBO Journal* **13**: 128–137.

811 **Schiestl FP, Johnson SD. 2013.** Pollinator-mediated evolution of floral signals. *Trends in*  
812 *Ecology & Evolution* **28**: 307–315.

813 **Schmitt AJ, Roy R, Klinkenberg PM, Jia M, Carter CJ. 2018.** The Octadecanoid Pathway,  
814 but Not COI1, Is Required for Nectar Secretion in Arabidopsis thaliana. *Frontiers in Plant*  
815 *Science* **9**: 1060.

816 **Schubert R, Dobritsch S, Gruber C, Hause G, Athmer B, Schreiber T, Marillonnet S,**  
817 **Okabe Y, Ezura H, Acosta IF, et al. 2019.** Tomato MYB21 Acts in Ovules to Mediate  
818 Jasmonate-Regulated Fertility. *The Plant Cell* **31**: 1043–1062.

819 **Shan X, Li Y, Yang S, Yang Z, Qiu M, Gao R, Han T, Meng X, Xu Z, Wang L, et al. 2020.**  
820 The spatio-temporal biosynthesis of floral flavonols is controlled by differential phylogenetic  
821 MYB regulators in Freesia hybrida. *New Phytologist* **228**: 1864–1879.

822 **Soltis DE, Chanderbali AS, Kim S, Buzgo M, Soltis PS. 2007.** The ABC Model and its  
823 Applicability to Basal Angiosperms. *Annals of Botany* **100**: 155–163.

824 **Song S, Qi T, Huang H, Ren Q, Wu D, Chang C, Peng W, Liu Y, Peng J, Xie D. 2011.** The  
825 Jasmonate-ZIM Domain Proteins Interact with the R2R3-MYB Transcription Factors MYB21  
826 and MYB24 to Affect Jasmonate-Regulated Stamen Development in Arabidopsis. *The Plant Cell*  
827 **23**: 1000–1013.

828 **Spitzer-Rimon B, Farhi M, Albo B, Cna'ani A, Zvi MMB, Masci T, Edelbaum O, Yu Y,**  
829 **Shklarman E, Ovadis M, et al. 2012.** The R2R3-MYB-Like Regulatory Factor EOBI, Acting  
830 Downstream of EOBI, Regulates Scent Production by Activating ODO1 and Structural Scent-  
831 Related Genes in Petunia. *The Plant Cell* **24**: 5089–5105.

832 **Spitzer-Rimon B, Marhevka E, Barkai O, Marton I, Edelbaum O, Masci T, Prathapani N-**  
833 **K, Shklarman E, Ovadis M, Vainstein A. 2010.** EOBII, a Gene Encoding a Flower-Specific  
834 Regulator of Phenylpropanoid Volatiles' Biosynthesis in Petunia. *The Plant Cell* **22**: 1961–1976.

835 **Streb S, Zeeman SC. 2012.** Starch Metabolism in Arabidopsis. *The Arabidopsis Book /*  
836 *American Society of Plant Biologists* **10**: e0160.

837 **Van Moerkercke A, Galván-Ampudia CS, Verdonk JC, Haring MA, Schuurink RC. 2012.**  
838 Regulators of floral fragrance production and their target genes in petunia are not exclusively  
839 active in the epidermal cells of petals. *Journal of Experimental Botany* **63**: 3157–3171.

840 **Vandenbussche M, Zethof J, Royaert S, Weterings K, Gerats T. 2004.** The duplicated B-class  
841 heterodimer model: whorl-specific effects and complex genetic interactions in *Petunia hybrida*  
842 flower development. *The Plant Cell* **16**: 741–754.

843 **Wang Y, Zhou L-J, Wang Y, Geng Z, Ding B, Jiang J, Chen S, Chen F. 2022.** An R2R3-  
844 MYB transcription factor CmMYB21 represses anthocyanin biosynthesis in color fading petals of  
845 chrysanthemum. *Scientia Horticulturae* **293**: 110674.

846 **Weirauch MT, Yang A, Albu M, Cote AG, Montenegro-Montero A, Drewe P, Najafabadi**  
847 **HS, Lambert SA, Mann I, Cook K, et al. 2014.** Determination and Inference of Eukaryotic  
848 Transcription Factor Sequence Specificity. *Cell* **158**: 1431–1443.

849 **Wu T, Hu E, Xu S, Chen M, Guo P, Dai Z, Feng T, Zhou L, Tang W, Zhan L, et al. 2021a.**  
850 clusterProfiler 4.0: A universal enrichment tool for interpreting omics data. *The Innovation* **2**:  
851 100141.

852 **Wu Z, Li T, Liu X, Yuan G, Hou H, Teng N. 2021b.** A novel R2R3-MYB transcription factor  
853 LIMYB305 from *Lilium longiflorum* plays a positive role in thermotolerance via activating heat-  
854 protective genes. *Environmental and Experimental Botany* **184**: 104399.

855 **Yang Z, Li Y, Gao F, Jin W, Li S, Kimani S, Yang S, Bao T, Gao X, Wang L. 2020.** MYB21  
856 interacts with MYC2 to control the expression of terpene synthase genes in flowers of *Freesia*  
857 *hybrida* and *Arabidopsis thaliana*. *Journal of Experimental Botany* **71**: 4140–4158.

858 **Yarahmadov T, Robinson S, Hanemian M, Pulver V, Kuhlemeier C. 2020.** Identification of  
859 transcription factors controlling floral morphology in wild *Petunia* species with contrasting  
860 pollination syndromes. *The Plant Journal* **104**: 289–301.

861 **Zhang C, Dai Z, Ferrier T, Matus JT. 2021a.** The grape MYB24 mediates the coordination of  
862 light-induced terpene and flavonol accumulation in response to berry anthocyanin sunscreen  
863 depletion. *Preprint bioRxiv*.

864 **Zhang X, He Y, Li L, Liu H, Hong G. 2021b.** Involvement of the R2R3-MYB transcription  
865 factor MYB21 and its homologs in regulating flavonol accumulation in *Arabidopsis* stamen.  
866 *Journal of Experimental Botany* **72**: 4319–4332.

867



868 **SUPPORTING INFORMATION**

869 The following Supporting information is available for this article.

870 **Fig. S1** Multiple sequence alignment of SG19 R2R3-MYB proteins.

871 **Fig. S2** Microsynteny analysis comparing genomic regions surrounding *EOB1* or *EOB2* in *P.*  
872 *axillaris* and *S. lycopersicum*.

873 **Fig. S3** Description of the different *Petunia axillaris* P floral developmental stages used in this  
874 study.

875 **Fig. S4** Construction of *eob1* and *eob2* mutant alleles by CRISPR-Cas9.

876 **Fig. S5** Observation of the internal floral organs of *eob2-1<sup>KO</sup>* and *eob2-2<sup>KO</sup>* flower buds.

877 **Fig. S6** The *eob2-3<sup>LofTAD</sup>* and *eob2-4<sup>LofTAD</sup>* are semi-dominant alleles.

878 **Fig. S7** *EOB1* and *EOB2* promoter sequences are highly divergent.

879 **Fig. S8** Additional phenotyping of *eob2-3<sup>LofTAD</sup>*.

880 **Fig. S9** Branches of WT, *eob2-1<sup>KO</sup>* and *eob2-2<sup>KO</sup>* before and after 1-MCP treatment.

881 **Fig. S10** *eob2-1<sup>KO</sup>* and *eob2-2<sup>KO</sup>* flowers after 1-MCP treatment, looked similar to *eob2-3<sup>LofTAD</sup>*  
882 and *eob2-4<sup>LofTAD</sup>*.

883 **Fig. S11** Percentage of genes with a 2kb promoter containing at least one putative R2R3-MYB  
884 SG19 binding site.

885 **Fig. S12** Model showing the direct activation of secondary metabolite related genes by *EOB2*.

886

887 **Table S1** Summary of protein-protein interactions involving members of the R2R3-MYB SG19  
888 reported in the literature.

889 **Table S2** Summary of the direct target genes of members of the R2R3-MYB SG19 reported in  
890 the literature.

891 **Table S3** gRNA sequences used to target *EOB1* and *EOB2*.

892 **Table S4** Sequence description of primers used for this work.

893 **Table S5** Description of the samples collected for the RNA sequencing experiment.

894 **Table S6** Description of the samples collected for the starch and carotenoid measurements.

895 **Table S7** From the T0 transgenic lines obtained by CRISPR-Cas9 to the final homozygous  
896 mutant lines used in this study.

897 **Table S8** Fraction of genes with a 2kb promoter containing at least one putative R2R3-MYB  
898 SG19 binding site.

899 **Table S9** Gene ID of genes used in this study.

900 **Method S1** Quantification of sesquiterpene accumulation in *Petunia* pistils and emission from  
901 tube by GC-MS.

902 **Method S2** Carotenoid extraction and quantification with an HPLC system.

903 **Method S3** Starch extraction and quantification with an HPLC system.

904

## 905 **FIGURE LEGENDS**

906

907 **Fig. 1 Analysis of the R2R3-MYB Subgroup 19 (SG19) family complexity and focus on *P.***  
908 ***axillaris* EOB1 and EOB2 members.**

909 **(a)** Phylogenetic analysis of members of the SG19 R2R3-MYB in *Arabidopsis thaliana* (At),  
910 *Solanum lycopersicum* (Sl), *Nicotiana tabacum* (Nt), *Petunia hybrida* (Ph) and *Petunia axillaris*  
911 (Pax). Numbers at nodes represent bootstrap values and scale bar indicates the number of amino  
912 acid substitutions per site. Gene functions reported in the literature are indicated by black squares  
913 in the associated table (flower opening, flower senescence, stamen development, nectary  
914 development, ovule development, pistil length, flavonol, terpene and scent production). **(b)**  
915 Diagram describing the SG19 R2R3-MYB protein structure with domain organization. The  
916 R2R3-MYB domain (RMD<sup>SG19</sup>) is represented in red and the C-terminal motif  
917 NyWS<sup>V</sup>/M<sup>E</sup>/D<sup>I</sup>/LW<sup>P</sup>/s which is a transcriptional activation domain (TAD) in blue. The RMD<sup>SG19</sup>  
918 is involved in DNA binding of specific target genes, protein-protein interactions (with repressor  
919 proteins such as DELLAs, JAZs or bHLHs) and contains a nuclear localization signal (NLS) (See  
920 Tables S1 and S2 for more details). The dashed line below the RMD<sup>SG19</sup> represents the position of  
921 the putative bipartite NLS. The R2R3-MYB domain binds DNA and the TAD activates the target  
922 genes. **(c)** Floral developmental stages, floral parts and pistil parts of *P. axillaris* used in this  
923 study. Scale bar = 1 cm. S1 to S10 = Stage 1 to Stage 10, more details about stages are available  
924 on Fig. S3. **(d)** RT-qPCR analysis of *EOB1* and *EOB2* expression in *P. axillaris* P. The different  
925 floral tissues have been dissected from open flower (S10). Stem = floral stem, BO = Basal ovary,  
926 AO = Apical ovary; D0-D4 = Number of days post anthesis. Relative expression values are  
927 means of three biological replicates with standard deviation, normalized against *ACT11* and  
928 *RAN1*. **(e)** RNA sequencing analysis of *EOB1* and *EOB2* expression in petal limb and basal  
929 ovaries (BO) at different stages (details are available in **Table S5**).

930

931 **Fig. 2 Generation of EOB2 domain-variants allowed to dissect and characterize EOB2**  
932 **domain functions during *P. axillaris* flower development.**

933 **(a)** DNA sequences of wild-type *EOB1* and *EOB2*. Exons are shown as grey boxes, solid lines  
934 represent introns. Position of the double gRNAs used to target *EOB1* (gRNA1 and gRNA2) and  
935 *EOB2* (gRNA3 and gRNA4) are indicated. **(b)** Diagrams of *EOB1* and *EOB2* wild-type (WT)  
936 proteins illustrating the R2R3-MYB domain (RMD<sup>SG19</sup>) and the transcriptional activation domain  
937 (TAD) with their respective amino acid regions, aligned with predicted proteins obtained after  
938 CRISPR-Cas9 mutagenesis. Boxes with dashed lines represent unrelated amino acid sequences  
939 compared to the wild type. Left: allele names. Right: The DNA column describes the deletions  
940 obtained in base pairs (bp) and the protein column predicts the associated protein length in amino  
941 acids (aa) followed by the predicted protein activities according to the domain composition (eob1-  
942 1, eob2-1, eob2-3, eob2-4) or protein conformation (eob2-2). **(c)** Diagrams of protein conformation  
943 and domains composition of *EOB1* and *EOB2* wild-type and mutant alleles sorted by knockout  
944 (KO) and loss-of-TAD (LofTAD) categories. **(d)** *EOB2* and eob2-2 protein structures prediction  
945 with AlphaFold, figure was drawn with PyMOL. **(e)** Pictures of WT, *eob1-1<sup>KO</sup>*, *eob2-1<sup>KO</sup>* and *eob2-3<sup>LofTAD</sup>*  
946 flower development over time. S2 flower buds were used at day 0. No visible phenotype  
947 between WT and *eob1-1<sup>KO</sup>*. Premature senescence observed in *eob2-1<sup>KO</sup>* (same phenotype for *eob2-2<sup>KO</sup>*)  
948 and juvenile flowers in *eob2-3<sup>LofTAD</sup>* (as well as *eob2-4<sup>LofTAD</sup>*). **(f)** Pictures of flower, ovary  
949 with nectary glands (NG) and stigma surface of WT, *eob1-1<sup>KO</sup>*, *eob2-1<sup>KO</sup>* and *eob2-3<sup>LofTAD</sup>* at stage  
950 5 (S5) and stage 10 (S10). Before S5, no differences observed between the different genotypes.  
951 After reaching S5, *eob2-1<sup>KO</sup>* and *eob2-2<sup>KO</sup>* stop growing and rapidly enter senescence. At S10,  
952 *eob2-3<sup>LofTAD</sup>* petals did not fully open, stigma surface and nectary were dry and immature compared  
953 to the WT or *eob1-1*. **(e)** and **(f)** scale bars are 1 cm for flowers and 1 mm for ovaries and stigmas.  
954

955 **Fig. 3 EOB2 is a regulator of EOB1.**

956 **(a)** Flower growth measurements of WT and crispr mutants from around 1 cm buds until  
957 senescence. Ten flowers per genotype were used for the analysis: WT, *eob1-1<sup>KO</sup>*, *eob2-1<sup>KO</sup>*, *eob2-2<sup>KO</sup>*,  
958 and *eob1-1<sup>KO</sup> eob2-2<sup>KO</sup>* double mutant. The black arrows indicate the first signs of  
959 senescence. The right panel represents the percentage of open flowers 16 weeks after germination  
960 (n = 100). **(b)** PTR-MS measurements for the major scent compounds, benzaldehyde and  
961 methylbenzoate, performed just before dark on 1 DPA flowers from WT and *eob1-1<sup>KO</sup>* plants (n =

962 15; error bar = SD; significant differences \*,  $P < 0.05$ ; Student's t-test). **(c)** RT-qPCR analysis of  
 963 *ODO1* and *EOB2* expression in WT and *eob1-1<sup>KO</sup>* limb at S10, 1DPA, just before dark (n = 3;  
 964 error bar = SD. **(d)** RNA sequencing analysis of *EOB1* expression in WT and *eob2-1<sup>KO</sup>* S5 petal  
 965 limb (n = 3; error bar = SD; significant differences \*,  $P < 0.05$ ; Student's t-test). **(e)** Schematic  
 966 representation of a *Petunia* plant showing the extraction of three leaf-disks in the infiltration area.  
 967 RT-qPCR analysis of *EOB1*, *EOB2* and *IGS* normalized expression in *Petunia axillaris* P leaves,  
 968 3 days after agroinfiltration with transient expression constructs (n = 4; error bar = SD;  
 969 significant differences \*,  $P < 0.05$ ; Student's t-test). *P35S::GFP* represents the negative control.  
 970 **(f)** Illustration showing a possible interaction between *EOB2* and the promoter of *EOB1*. *EOB1*  
 971 and *EOB2* promoter sequence analysis (1000bp before the ATG) revealed the presence of a  
 972 putative SG19 MYB-binding site 450bp before the START codon of *EOB1*.

973

974 **Fig. 4 Different organs impacted in their maturation in *eob2-3<sup>LofTAD</sup>* mutants.**

975 **(a)** Pictures of WT (top row) and *eob2-3<sup>LofTAD</sup>* (bottom row) flowers at stage 10 (S10). Side view,  
 976 top view, bottom view, stigma surface, stigma surface 24h after pollination of freshly opened  
 977 flowers and close up of the nectary gland. Scale bar is 1 cm. **(b)** Pistil pictures of WT and *eob2-*  
 978 *3<sup>LofTAD</sup>*, 5 days after S3. Left: no petal removal (S10). Right: with petal removal performed at  
 979 around S3 (w/o). Twisted styles in *eob2-3<sup>LofTAD</sup>* are due to petal mechanical constraints. **(c)**  
 980 Capsules one month after pollination. The mean number of seeds per capsule is indicated (n = 6).  
 981 No seeds in the *eob2-3<sup>LofTAD</sup>* capsule without stigma exudate. **(d)** Side view of ovaries with carpel  
 982 wall removed, comparable number of ovules was observed. **(e)** Two weeks after pollination the  
 983 style detached from the fruit/capsule of WT while persisting in *eob2-3<sup>LofTAD</sup>*. **(f)** to **(m)** WT is  
 984 represented in white and *eob2-3<sup>LofTAD</sup>* in dark grey (error bar = SD, except (k) and (l) where error  
 985 bar = SE; significant differences \*,  $P < 0.05$ ; Student's t-test). **(f)** Petal morphological  
 986 measurements at S10: petal tube length, petal opening angle and petal limb area (n = 12). **(g)**  
 987 Nectar volume measurements at S10 (n = 20). **(h)** Carotenoid content from nectary at S10. **(i)**  
 988 PTR-MS measurements of the two main floral volatiles benzenoid/phenylpropanoid (FVBP) (n =  
 989 15). **(j)** RNA-seq of *ODO1* and *EOB1* expression in WT and *eob2-3<sup>LofTAD</sup>* limb at S10. **(k)**  
 990 Terpene volatiles (*TPSI* products) emitted from WT and *eob2-3<sup>LofTAD</sup>* petal tubes (n = 5). **(l)**  
 991 Terpene volatiles accumulated on stigmas during anthesis (S9) (n = 4). **(m)** RT-qPCR of *TPSI*  
 992 from petal tube at S10.

993

994 **Fig. 5 Premature production of ethylene by flower buds is responsible for the knockout**  
995 **flower senescence phenotype.**

996 **(a)** RNA-seq experiment summary. Right: White triangles show the petal limb tissue part from S5  
997 buds collected for the RNA-seq experiment (just before the first signs of senescence for *eob2-*  
998 *I<sup>KO</sup>*). Middle: pie charts showing the proportion of DEGs in the *P. axillaris* transcriptome (total of  
999 32768 genes). Significant DEGs = log<sub>2</sub>FC >1 or < -1 and p-adjusted value < 0.01. Left:  
1000 Comparison of S5 limb total DEGs from *eob2-I<sup>KO</sup>* vs WT and *eob2-3<sup>LofTAD</sup>* vs WT. **(b)** Gene  
1001 ontology (GO) term enrichment analysis of specific up-regulated genes in *eob2-I<sup>KO</sup>*. **(c)** RNA-seq  
1002 results of genes belonging to *ACS* and *ACO* multi-gene families encoding for enzymes of the  
1003 ethylene biosynthetic pathway. Only genes from the family expressed in either WT or *eob2-I* are  
1004 shown (*ACS* 8/22 and *ACO* 6/13) (see **Table S9** for gene ID). Error bar = SD. **(d)** Detection of  
1005 ethylene released from WT and *eob2-I<sup>KO</sup>* S5 full flower buds, S5 dissected petal or S5 dissected  
1006 pistil, quantified using a laser-based photoacoustic ethylene sensor (n = 30 for WT and n = 45 for  
1007 *eob2-I<sup>KO</sup>*; error bar = SE; significant differences \*, *P*<0.05; Student's t-test). Mutant samples  
1008 were collected before the first signs of senescence, when the petal tips were still rigid. **(e)** Side  
1009 view of flowers of WT, *eob2-I<sup>KO</sup>* and *eob2-3<sup>LofTAD</sup>* with or without 1-MCP treatment. Partial  
1010 rescue of the *eob2-I<sup>KO</sup>* phenotype was observed. Scale bars = 1 cm.

1011

1012 **Fig. 6 EOB2 activates the expression of common targets in two different floral organs.**

1013 **(a)** RNA-seq experiment summary. Top: limb and basal ovary tissues collected just before dark at  
1014 S5 and S10 for the RNA-seq experiment. Bottom: Number of DEGs between *eob2-3<sup>LofTAD</sup>* and  
1015 WT. **(b)** The graph corresponds to the difference in fraction of genes (up vs all / down vs all) with  
1016 a 2kb promoter containing at least one putative R2R3-MYB SG19 binding site (matrix  
1017 MA1408.1 (*FaEOBII*)). Similar results were obtained with MA1037.1 (*AtMYB24*) (**Table S8**). **(c)**  
1018 Summary of overlaps between down-regulated genes (*eob2-3<sup>LofTAD</sup>*<WT) in limb and nectary at  
1019 stages S5 and S10. **(d)** Table showing the expression data in limb and nectary at S10 of a  
1020 selection of 11 genes over a total of 60 (from **Fig. 6b**). n.r.c., normalized read counts, L2FC,  
1021 Log<sub>2</sub> fold change. The presence of a R2R3-MYB SG19 binding site in 2kb promoter was  
1022 predicted using FIMO. Motifs with grey nucleotides should also be recognized by SG19 proteins.  
1023 Emission Of Benzenoids 1 (EOB1), Chorismate Mutase 1 (CM1), Benzoic acid/Salicylic acid

1024 carboxyl MethylTransferase (BSMT), Eugenol Synthase (EGS), Isoeugenol Synthase (IGS).  
1025 Carotenoid related: ζ-carotene isomerase (Z-ISO), ζ-carotene desaturase (ZDS), Lycopene Beta  
1026 Cyclase (LCY B), Carotenoid cleavage dioxygenase (CCD). See **Table S9** for gene ID.

1027  
1028 **Fig. 7 Carbohydrate metabolism is disrupted in *eob2-3<sup>LofTAD</sup>* nectary and limb.**  
1029 **(a)** GO terms from down-regulated genes co-enriched in *eob2-3<sup>LofTAD</sup>* limb and nectary at S5 and  
1030 S10 (pvalue<0.005). **(b)** RNA-seq result of *BETA-AMYLASE (BAM)* in nectary and limb at S10.  
1031 See **Table S9** for gene ID. **(c)** Simplified representation of the carbohydrate metabolism pathway  
1032 and the derived primary and secondary metabolites (blue). PYR: pyruvate, PEP:  
1033 phosphoenolpyruvate, E4P: erythrose-4-phosphate, Rubisco: ribulose-1,5-bisphosphate  
1034 carboxylase/oxygenase and TCA cycle: tricarboxylic acid cycle, also known as the Krebs cycle.  
1035 **(d)** and **(e)** Visualization of starch in nectaries and cleared petal (S5 and S10) by staining with  
1036 Lugol's solution. **(f)** Adaxial epidermal cell peeling from petal limb at S10. Left: Lugol's  
1037 staining. Right: differential interference contrast (DIC) observation. Arrows indicate the starch  
1038 granules inside the limb epidermal cells. Scale bar is 30 μm. Basal epidermal cell area (μm<sup>2</sup>) of  
1039 petal limb at S10 (n = 90 cells; error bar = SD; significant differences \*, *P*<0.05; Student's t-  
1040 test). **(g)** Starch content in WT and *eob2-3<sup>LofTAD</sup>* nectary and limb tissues at different stages. The  
1041 black arrow indicates the tendency towards an accumulation of starch in *eob2-3<sup>LofTAD</sup>* limb S10  
1042 compared to the WT (n = 3; error bar = SD; significant differences \*, *P*<0.05; ns, non-  
1043 significance; Student's t-test).

1044  
1045 **Fig. 8 One gene, two mutations, contrasting phenotypes.**  
1046 Model to illustrate EOB2 multi-functionality. The knockout (KO) lines and LofTAD lines do not  
1047 present the same floral phenotype, while both lines are unable to activate target genes. This is the  
1048 proof that EOB2 is involved in other functions. Direct targets are most likely related to  
1049 maturation-related genes like the secondary metabolism related genes, while indirect targets are  
1050 probably senescence-related proteins/genes.

1051

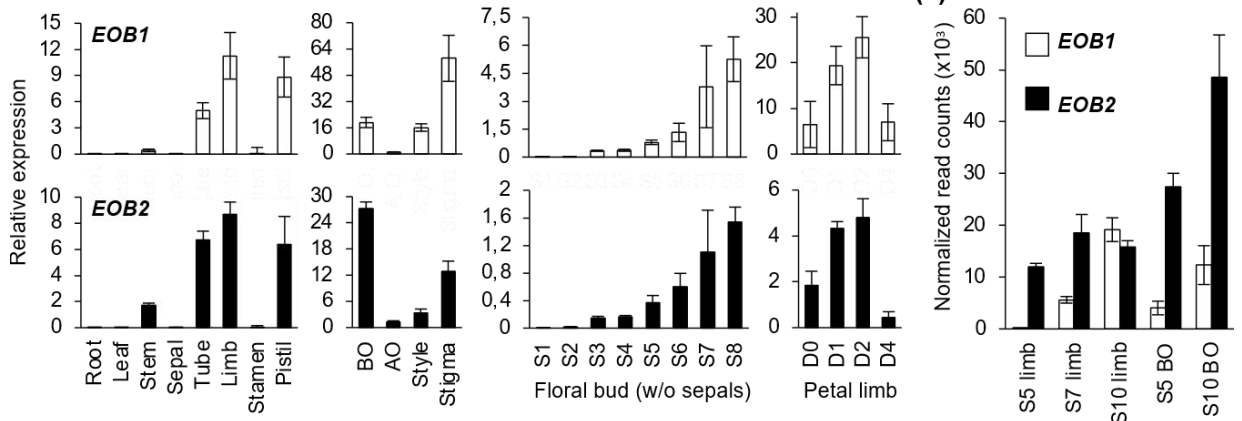
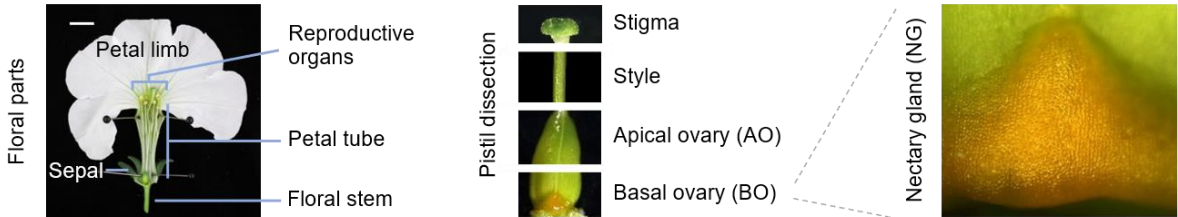
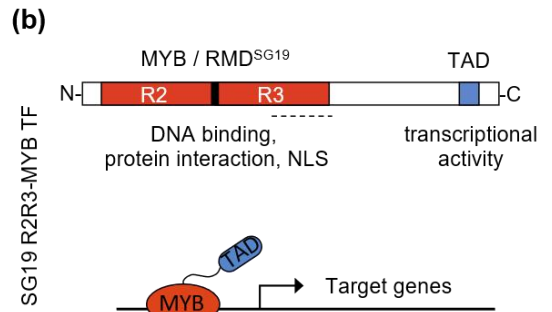
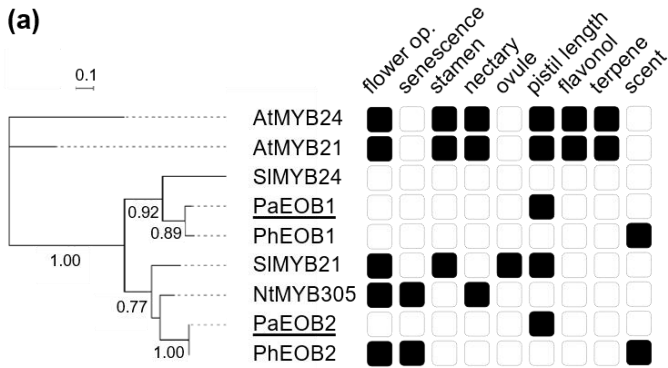


**Fig. 1 Analysis of the R2R3-MYB Subgroup 19 (SG19) family complexity and focus on *P. axillaris* EOB1 and EOB2 members.**

**(a)** Phylogenetic analysis of members of the SG19 R2R3-MYB in *Arabidopsis thaliana* (At), *Solanum lycopersicum* (Sl), *Nicotiana tabacum* (Nt), *Petunia hybrida* (Ph) and *Petunia axillaris* (Pax). Numbers at nodes represent bootstrap values and scale bar indicates the number of amino acid substitutions per site. Gene functions reported in the literature are indicated by black squares in the associated table (flower opening, flower senescence, stamen development, nectary development, ovule development, pistil length, flavonol, terpene and scent production).

**(b)** Diagram describing the SG19 R2R3-MYB protein structure with domain organization. The R2R3-MYB domain (RMD<sup>SG19</sup>) is represented in red and the C-terminal motif NyWS<sup>V</sup>/<sub>M</sub><sup>E</sup>/<sub>D</sub>D<sup>I</sup>/<sub>L</sub>W<sup>P</sup>/<sub>S</sub> which is a transcriptional activation domain (TAD) in blue. The RMD<sup>SG19</sup> is involved in DNA binding of specific target genes, protein-protein interactions (with repressor proteins such as DELLAs, JAZs or bHLHs) and contains a nuclear localization signal (NLS) (See Tables S1 and S2 for more details). The dashed line below the RMD<sup>SG19</sup> represents the position of the putative bipartite NLS. The R2R3-MYB domain binds DNA and the TAD activates the target genes.

**(c)** Floral developmental stages, floral parts and pistil parts of *P. axillaris* used in this study. Scale bar = 1 cm. S1 to S10 = Stage 1 to Stage 10, more details about stages are available on Fig. S3.

**(d)** RT-qPCR analysis of *EOB1* and *EOB2* expression in *P. axillaris* P. The different floral tissues have been dissected from open flower (S10). Stem = floral stem, BO = Basal ovary, AO = Apical ovary; D0-D4 = Number of days post anthesis. Relative expression values are means of three biological replicates with standard deviation, normalized against *ACT11* and *RAN1*.

**(e)** RNA sequencing analysis of *EOB1* and *EOB2* expression in petal limb and basal ovaries (BO) at different stages (details are available in **Table S5**).



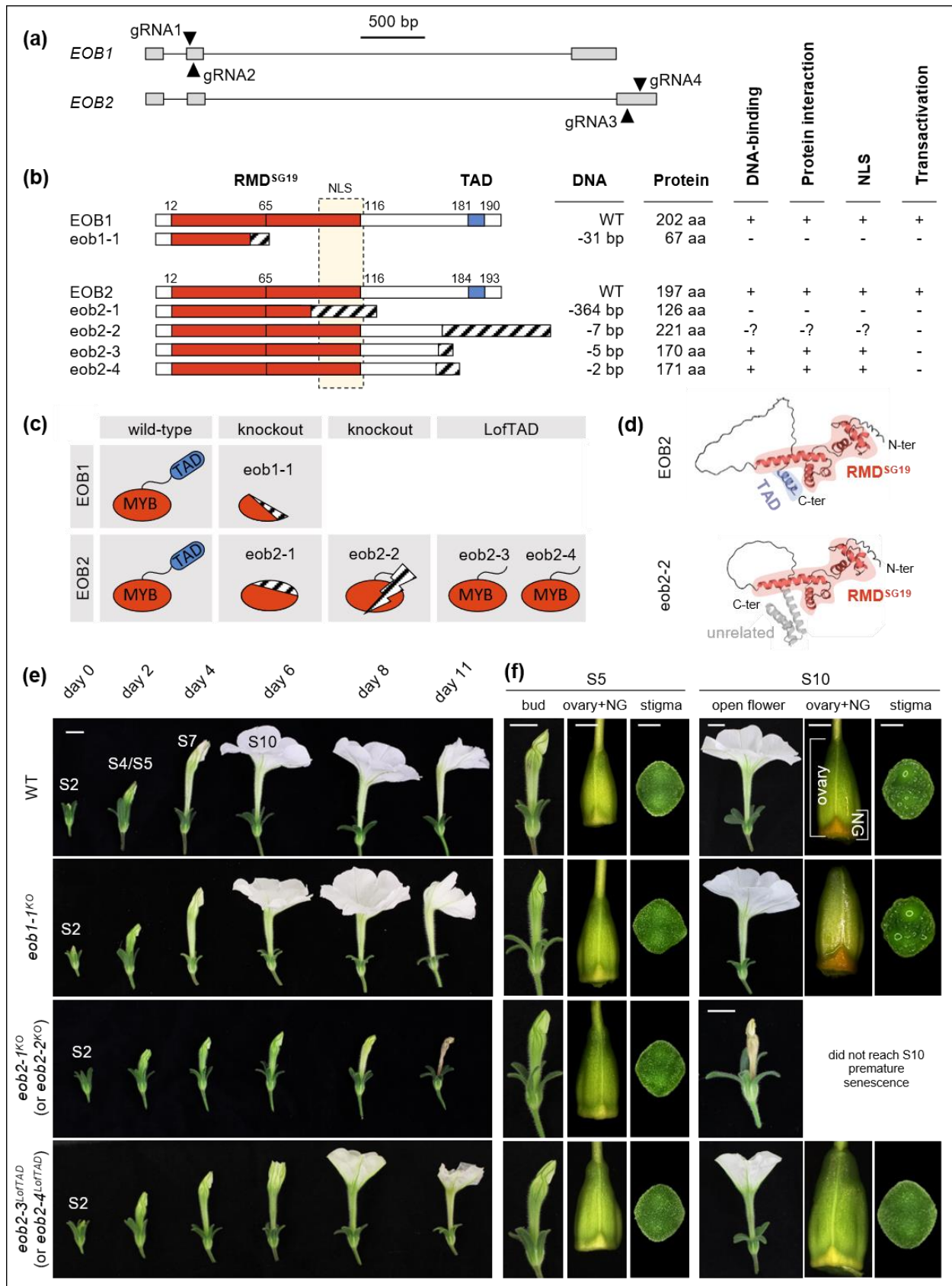


**Fig. 2 Generation of EOB2 domain-variants allowed to dissect and characterize EOB2 domain functions during *P. axillaris* flower development.**

(a) DNA sequences of wild-type *EOB1* and *EOB2*. Exons are shown as grey boxes, solid lines represent introns. Position of the double gRNAs used to target *EOB1* (gRNA1 and gRNA2) and *EOB2* (gRNA3 and gRNA4) are indicated. (b) Diagrams of *EOB1* and *EOB2* wild-type (WT) proteins illustrating the R2R3-MYB domain (RMD<sup>SG19</sup>) and the transcriptional activation domain (TAD) with their respective amino acid regions, aligned with predicted proteins obtained after CRISPR-Cas9 mutagenesis. Boxes with dashed lines represent unrelated amino acid sequences compared to the wild type. Left: allele names. Right: The DNA column describes the deletions obtained in base pairs (bp) and the protein column predicts the associated protein length in amino acids (aa) followed by the predicted protein activities according to the domain composition (eob1-1, eob2-1, eob2-3, eob2-4) or protein conformation (eob2-2). (c) Diagrams of protein conformation and domains composition of *EOB1* and *EOB2* wild-type and mutant alleles sorted by knockout (KO) and loss-of-TAD (LofTAD) categories. (d) *EOB2* and eob2-2 protein structures prediction with AlphaFold, figure was drawn with PyMOL. (e) Pictures of WT, *eob1-1<sup>KO</sup>*, *eob2-1<sup>KO</sup>* and *eob2-3<sup>LofTAD</sup>* flower development over time. S2 flower buds were used at day 0. No visible phenotype between WT and *eob1-1<sup>KO</sup>*. Premature senescence observed in *eob2-1<sup>KO</sup>* (same phenotype for *eob2-2<sup>KO</sup>*) and juvenile flowers in *eob2-3<sup>LofTAD</sup>* (as well as *eob2-4<sup>LofTAD</sup>*). (f) Pictures of flower, ovary with nectary glands (NG) and stigma surface of WT, *eob1-1<sup>KO</sup>*, *eob2-1<sup>KO</sup>* and *eob2-3<sup>LofTAD</sup>* at stage 5 (S5) and stage 10 (S10). Before S5, no differences observed between the different genotypes. After reaching S5, *eob2-1<sup>KO</sup>* and *eob2-2<sup>KO</sup>* stop growing and rapidly enter senescence. At S10, *eob2-3<sup>LofTAD</sup>* petals did not fully open, stigma surface and nectary were dry and immature compared to the WT or *eob1-1*. (e) and (f) scale bars are 1 cm for flowers and 1 mm for ovaries and stigmas.

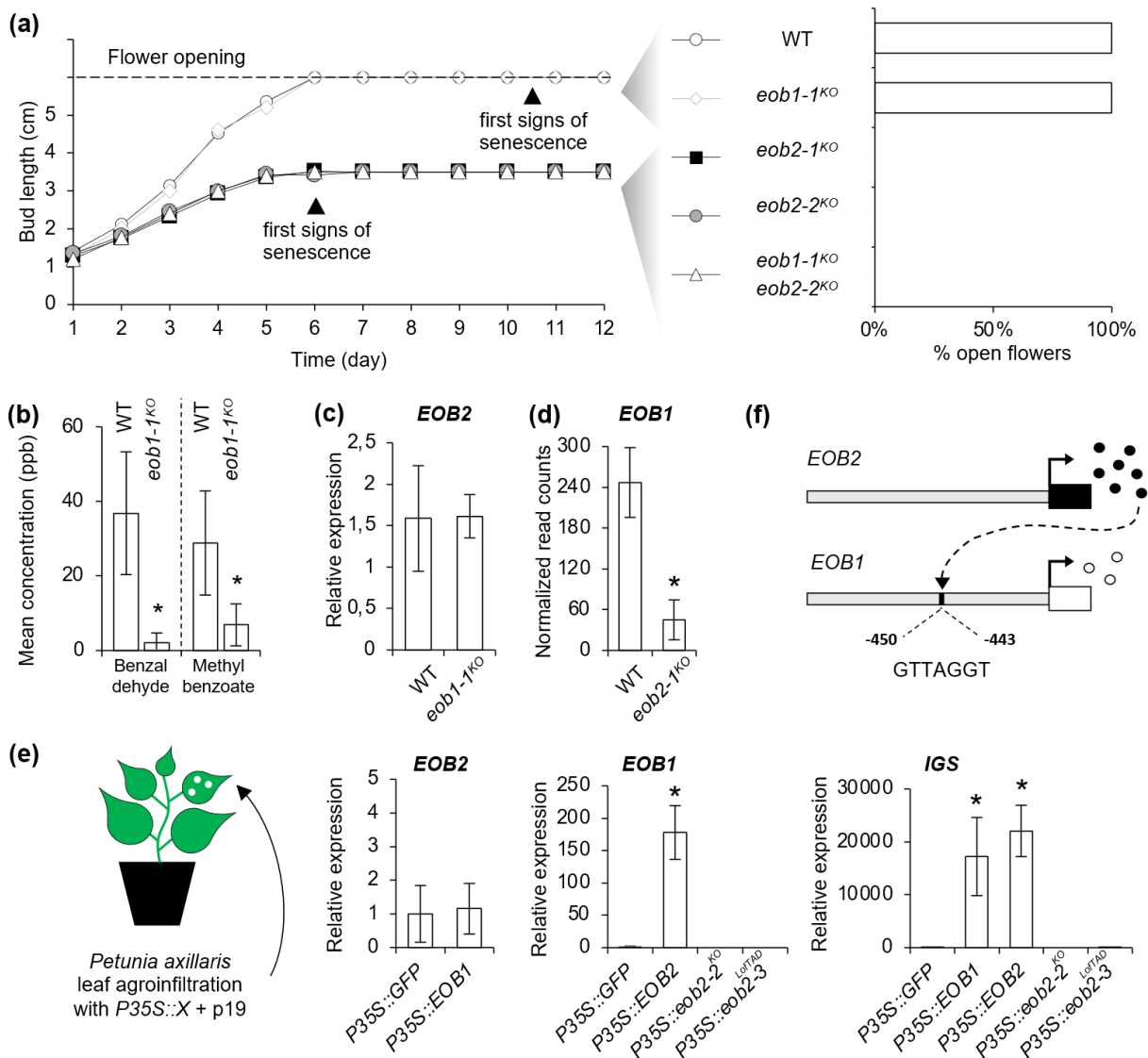


### Fig. 3 EOB2 is a regulator of EOB1.

**(a)** Flower growth measurements of WT and crispr mutants from around 1 cm buds until senescence. Ten flowers per genotype were used for the analysis: WT, *eob1-1<sup>KO</sup>*, *eob2-1<sup>KO</sup>*, *eob2-2<sup>KO</sup>*, and *eob1-1<sup>KO</sup> eob2-2<sup>KO</sup>* double mutant. The black arrows indicate the first signs of senescence. The right panel represents the percentage of open flowers 16 weeks after germination (n = 100). **(b)** PTR-MS measurements for the major scent compounds, benzaldehyde and methylbenzoate, performed just before dark on 1 DPA flowers from WT and *eob1-1<sup>KO</sup>* plants (n = 15; error bar = SD; significant differences \*, *P*<0.05; Student's t-test). **(c)** RT-qPCR analysis of *ODO1* and *EOB2* expression in WT and *eob1-1<sup>KO</sup>* limb at S10, 1DPA, just before dark (n = 3; error bar = SD). **(d)** RNA sequencing analysis of *EOB1* expression in WT and *eob2-1<sup>KO</sup>* S5 petal limb (n = 3; error bar = SD; significant differences \*, *P*<0.05; Student's t-test). **(e)** Schematic representation of a *Petunia axillaris* leaf agroinfiltration with P35S::X + p19. RT-qPCR analysis of *EOB1*, *EOB2* and *IGS* normalized expression in *Petunia axillaris* P leaves, 3 days after agroinfiltration with transient expression constructs (n = 4; error bar = SD; significant differences \*, *P*<0.05; Student's t-test). P35S::GFP represents the negative control. **(f)** Illustration showing a possible interaction between *EOB2* and the promoter of *EOB1*. *EOB1* and *EOB2* promoter sequence analysis (1000bp before the ATG) revealed the presence of a putative SG19 MYB-binding site 450bp before the START codon of *EOB1*.

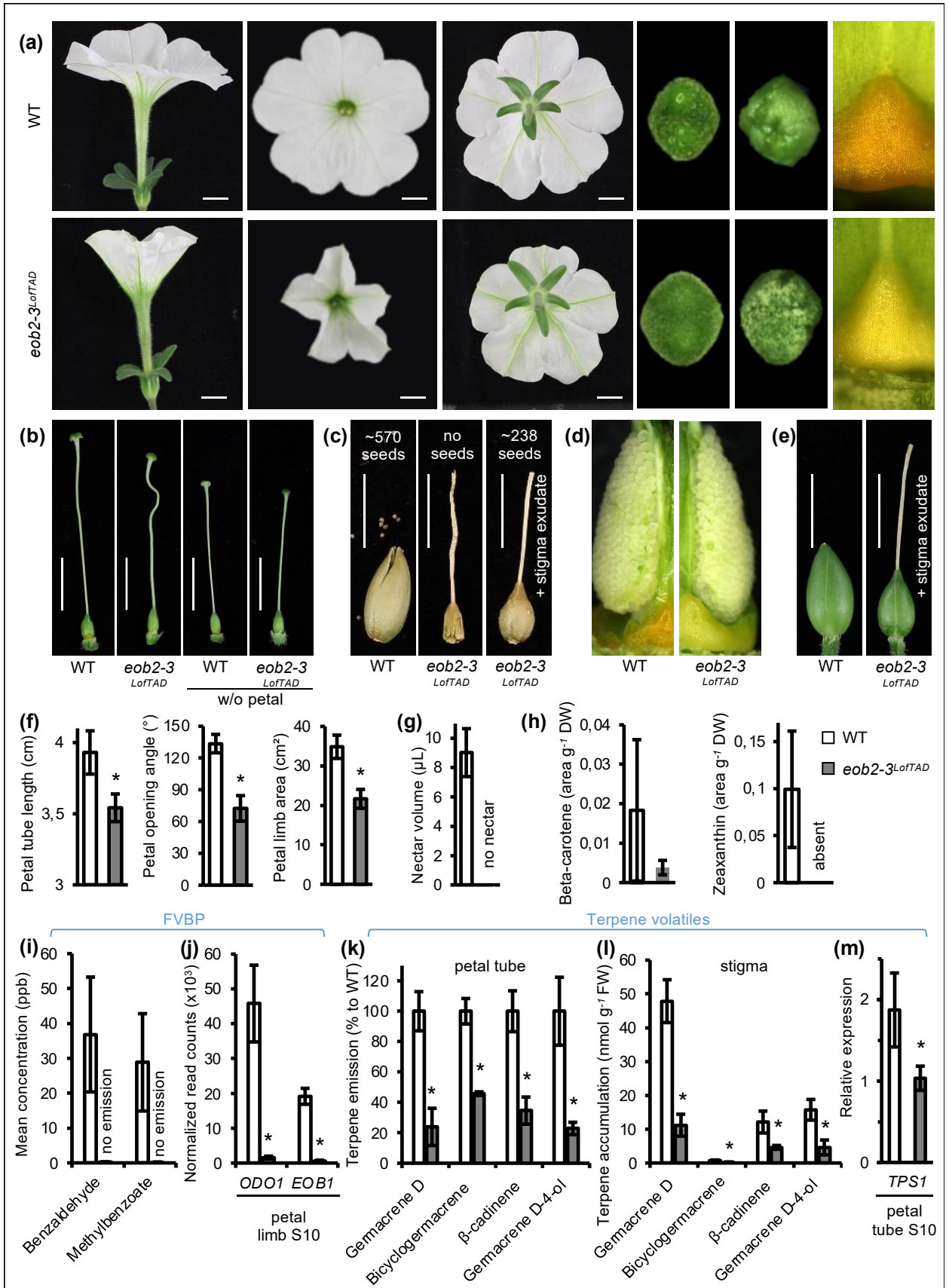


**Fig. 4 Different organs impacted in their maturation in *eob2-3<sup>LofTAD</sup>* mutants.**

(a) Pictures of WT (top row) and *eob2-3<sup>LofTAD</sup>* (bottom row) flowers at stage 10 (S10). Side view, top view, bottom view, stigma surface, stigma surface 24h after pollination of freshly opened flowers and close up of the nectary gland. Scale bar is 1 cm. (b) Pistil pictures of WT and *eob2-3<sup>LofTAD</sup>*, 5 days after S3. Left: no petal removal (S10). Right: with petal removal performed at around S3 (w/o). Twisted styles in *eob2-3<sup>LofTAD</sup>* are due to petal mechanical constraints. (c) Capsules one month after pollination. The mean number of seeds per capsule is indicated (n = 6). No seeds in the *eob2-3<sup>LofTAD</sup>* capsule without stigma exudate. (d) Side view of ovaries with carpel wall removed, comparable number of ovules was observed. (e) Two weeks after pollination the style detached from the fruit/capsule of WT while persisting in *eob2-3<sup>LofTAD</sup>*. (f) to (m) WT is represented in white and *eob2-3<sup>LofTAD</sup>* in dark grey (error bar = SD, except (k) and (l) where error bar = SE; significant differences \*,  $P < 0.05$ ; Student's t-test). (f) Petal morphological measurements at S10: petal tube length, petal opening angle and petal limb area (n = 12). (g) Nectar volume measurements at S10 (n = 20). (h) Carotenoid content from nectary at S10. (i) PTR-MS measurements of the two main floral volatiles benzenoid/phenylpropanoid (FVBP) (n = 15). (j) RNA-seq of *ODO1* and *EOB1* expression in WT and *eob2-3<sup>LofTAD</sup>* limb at S10. (k) Terpene volatiles (*TPS1* products) emitted from WT and *eob2-3<sup>LofTAD</sup>* petal tubes (n = 5). (l) Terpene volatiles accumulated on stigmas during anthesis (S9) (n = 4). (m) RT-qPCR of *TPS1* from petal tube at S10.

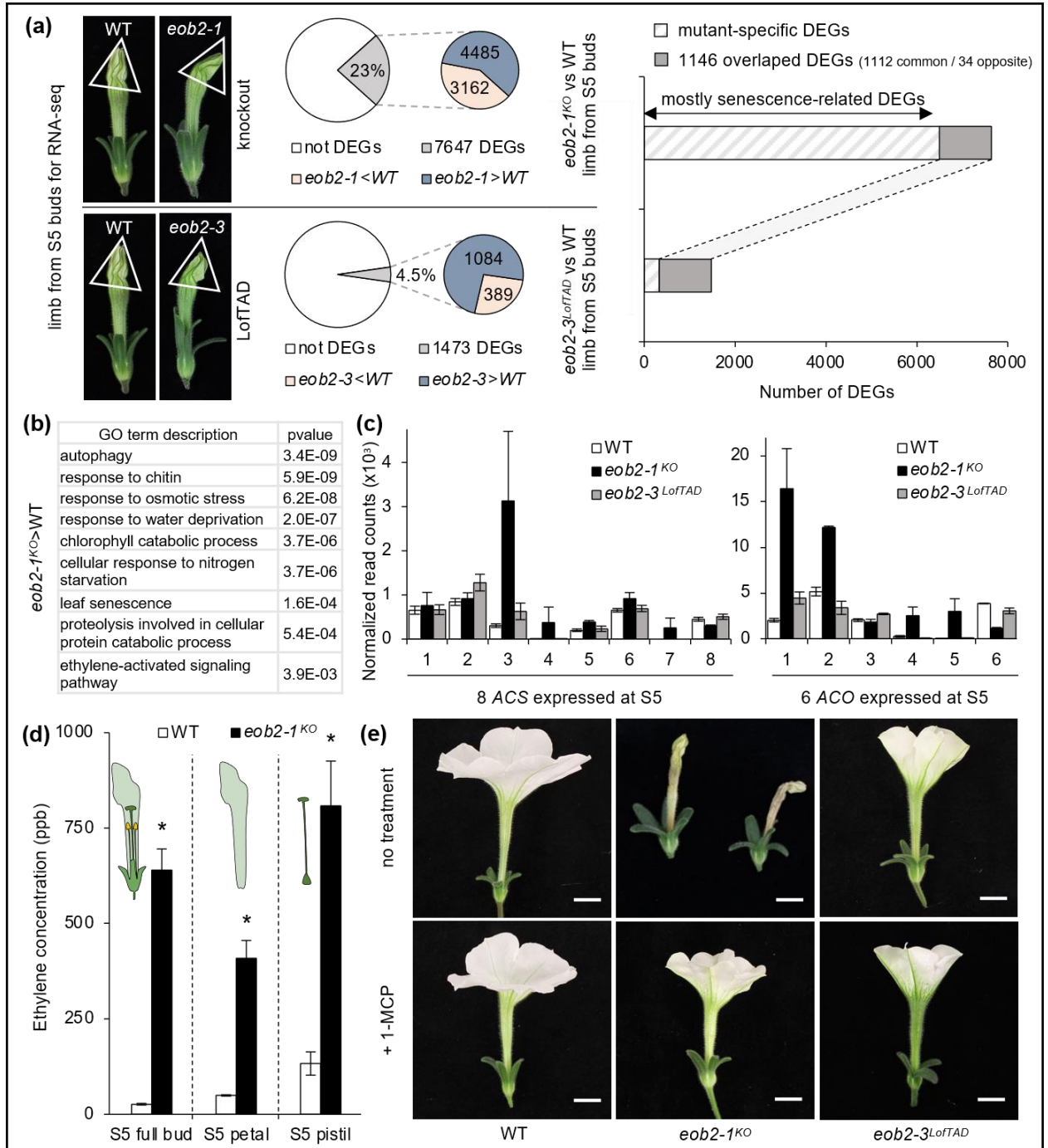


**Fig. 5 Premature production of ethylene by flower buds is responsible for the knockout flower senescence phenotype.**

**(a)** RNA-seq experiment summary. Right: White triangles show the petal limb tissue part from S5 buds collected for the RNA-seq experiment (just before the first signs of senescence for *eob2-1<sup>KO</sup>*). Middle: pie charts showing the proportion of DEGs in the *P. axillaris* transcriptome (total of 32768 genes). Significant DEGs =  $\log_2FC > 1$  or  $< -1$  and p-adjusted value  $< 0.01$ . Left: Comparison of S5 limb total DEGs from *eob2-1<sup>KO</sup>* vs WT and *eob2-3<sup>LofTAD</sup>* vs WT. **(b)** Gene ontology (GO) term enrichment analysis of specific up-regulated genes in *eob2-1<sup>KO</sup>*. **(c)** RNA-seq results of genes belonging to ACS and ACO multi-gene families encoding for enzymes of the ethylene biosynthetic pathway. Only genes from the family expressed in either WT or *eob2-1* are shown (ACS 8/22 and ACO 6/13) (see **Table S9** for gene ID). Error bar = SD. **(d)** Detection of ethylene released from WT and *eob2-1<sup>KO</sup>* S5 full flower buds, S5 dissected petal or S5 dissected pistil, quantified using a laser-based photoacoustic ethylene sensor (n = 30 for WT and n = 45 for *eob2-1<sup>KO</sup>*; error bar = SE; significant differences \*,  $P < 0.05$ ; Student's t-test). Mutant samples were collected before the first signs of senescence, when the petal tips were still rigid. **(e)** Side view of flowers of WT, *eob2-1<sup>KO</sup>* and *eob2-3<sup>LofTAD</sup>* with or without 1-MCP treatment. Partial rescue of the *eob2-1<sup>KO</sup>* phenotype was observed. Scale bars = 1 cm.



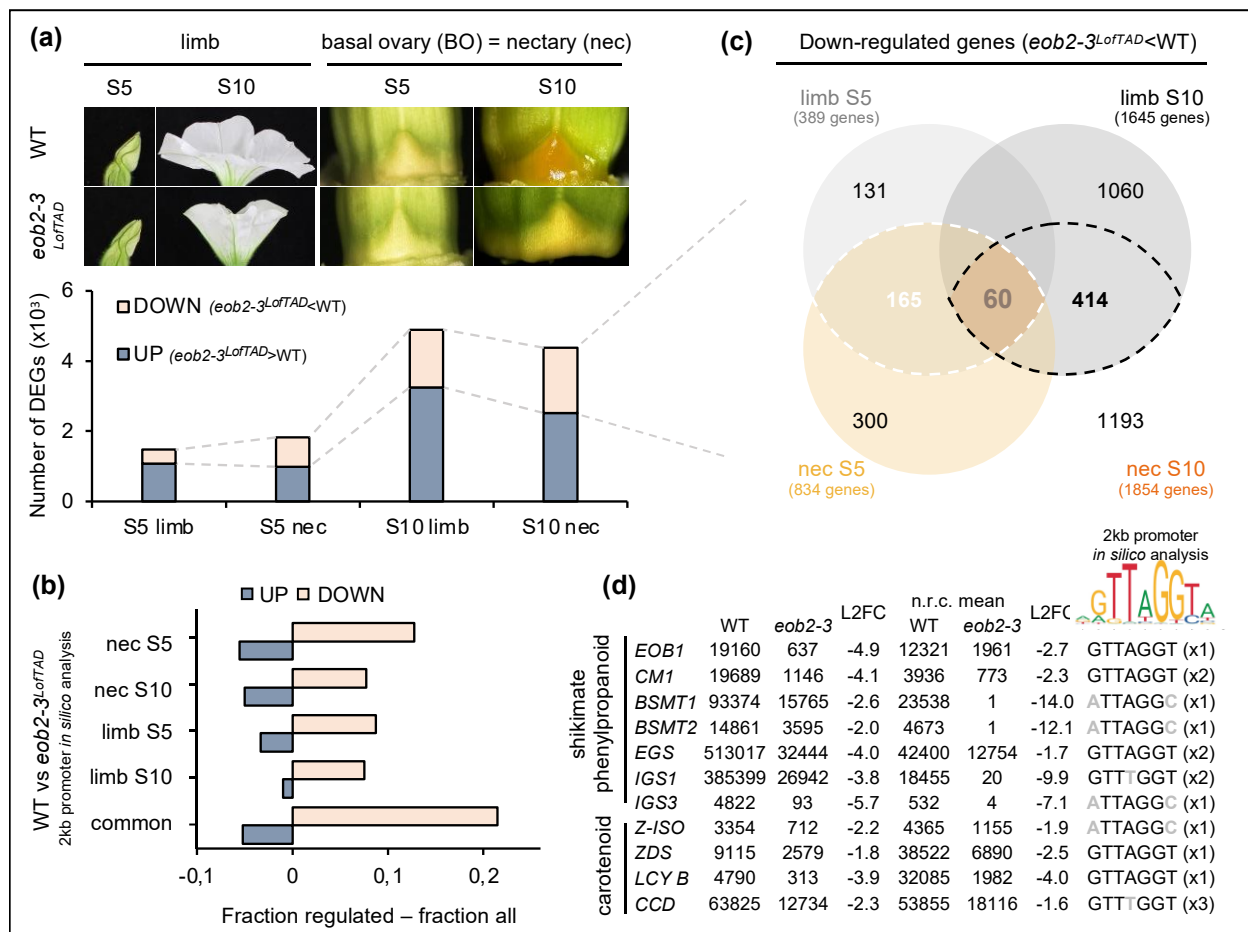


**Fig. 6 EOB2 activates the expression of common targets in two different floral organs.**

**(a)** RNA-seq experiment summary. Top: limb and basal ovary tissues collected just before dark at S5 and S10 for the RNA-seq experiment. Bottom: Number of DEGs between *eob2-3<sup>LoFTAD</sup>* and WT. **(b)** The graph corresponds to the difference in fraction of genes (up vs all / down vs all) with a 2kb promoter containing at least one putative R2R3-MYB SG19 binding site (matrix MA1408.1 (*FaEOBII*)). Similar results were obtained with MA1037.1 (*AtMYB24*) (Table S8). **(c)** Summary of overlaps between down-regulated genes (*eob2-3<sup>LoFTAD</sup><WT*) in limb and nectary at stages S5 and S10. **(d)** Table showing the expression data in limb and nectary at S10 of a selection of 11 genes over a total of 60 (from Fig. 6b). n.r.c., normalized read counts, L2FC, Log2 fold change. The presence of a R2R3-MYB SG19 binding site in 2kb promoter was predicted using FIMO. Motifs with grey nucleotides should also be recognized by SG19 proteins. Emission Of Benzenoids 1 (EOB1), Chorismate Mutase 1 (CM1), Benzoic acid/Salicylic acid carboxyl MethylTransferase (BSMT), Eugenol Synthase (EGS), Isoeugenol Synthase (IGS). Carotenoid related: ζ-carotene isomerase (Z-ISO), ζ-carotene desaturase (ZDS), Lycopene Beta Cyclase (LCY B), Carotenoid cleavage dioxygenase (CCD). See Table S9 for gene ID.



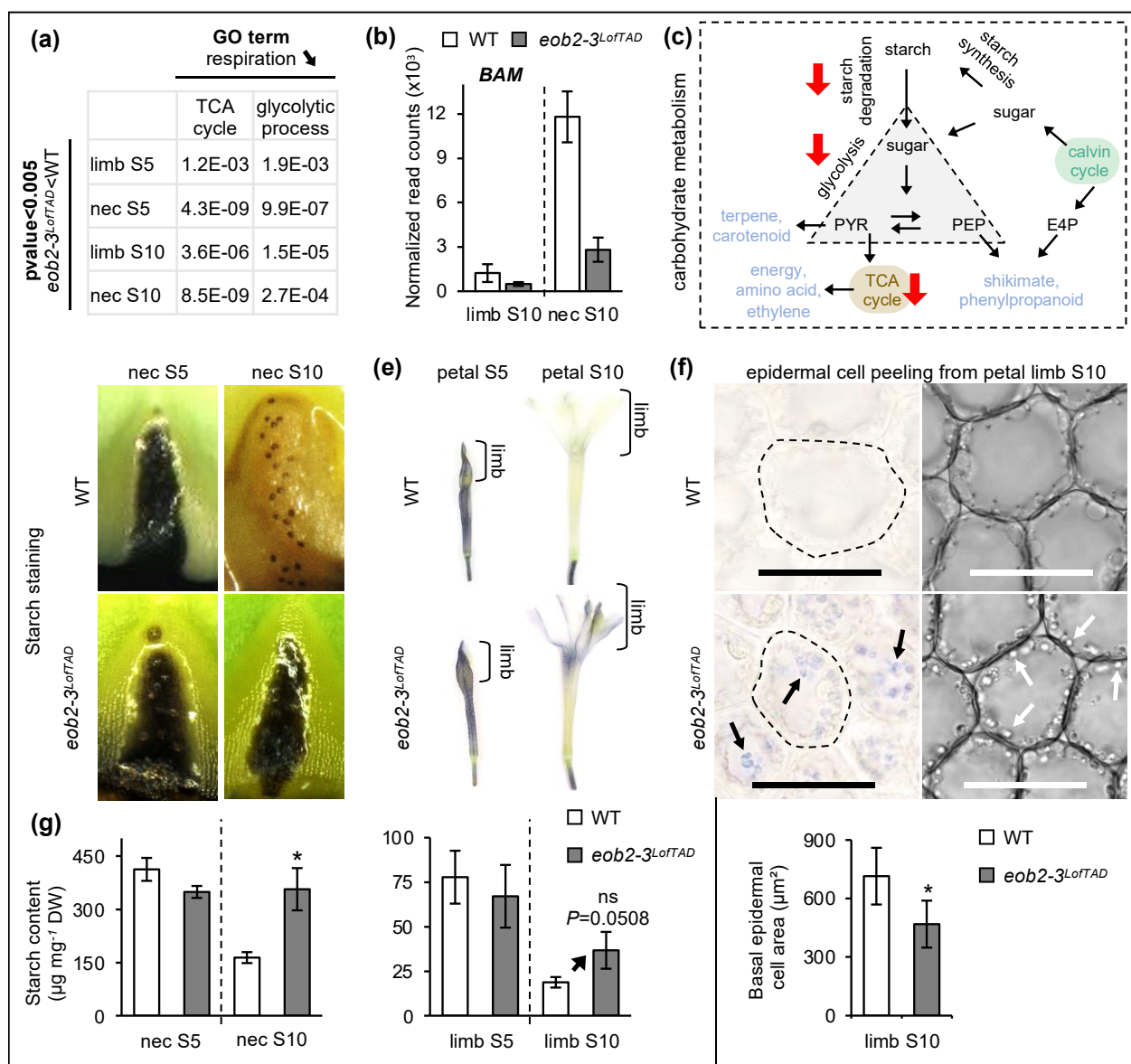


**Fig. 7 Carbohydrate metabolism is disrupted in *eob2-3<sup>LofTAD</sup>* nectary and limb.**

**(a)** GO terms from down-regulated genes co-enriched in *eob2-3<sup>LofTAD</sup>* limb and nectary at S5 and S10 (*p*value < 0.005). **(b)** RNA-seq result of *BETA-AMYLASE* (*BAM*) in nectary and limb at S10. See **Table S9** for gene ID. **(c)** Simplified representation of the carbohydrate metabolism pathway and the derived primary and secondary metabolites (blue). PYR: pyruvate, PEP: phosphoenolpyruvate, E4P: erythrose-4-phosphate, Rubisco: ribulose-1,5-bisphosphate carboxylase/oxygenase and TCA cycle: tricarboxylic acid cycle, also known as the Krebs cycle. **(d)** and **(e)** Visualization of starch in nectaries and cleared petal (S5 and S10) by staining with Lugol's solution. **(f)** Adaxial epidermal cell peeling from petal limb at S10. Left: Lugol's staining. Right: differential interference contrast (DIC) observation. Arrows indicate the starch granules inside the limb epidermal cells. Scale bar is 30  $\mu$ m. Basal epidermal cell area ( $\mu$ m<sup>2</sup>) of petal limb at S10 (n = 90 cells; error bar = SD; significant differences \*, *P* < 0.05; Student's t-test). **(g)** Starch content in WT and *eob2-3<sup>LofTAD</sup>* nectary and limb tissues at different stages. The black arrow indicates the tendency towards an accumulation of starch in *eob2-3<sup>LofTAD</sup>* limb S10 compared to the WT (n = 3; error bar = SD; significant differences \*, *P* < 0.05; ns, non-significance; Student's t-test).

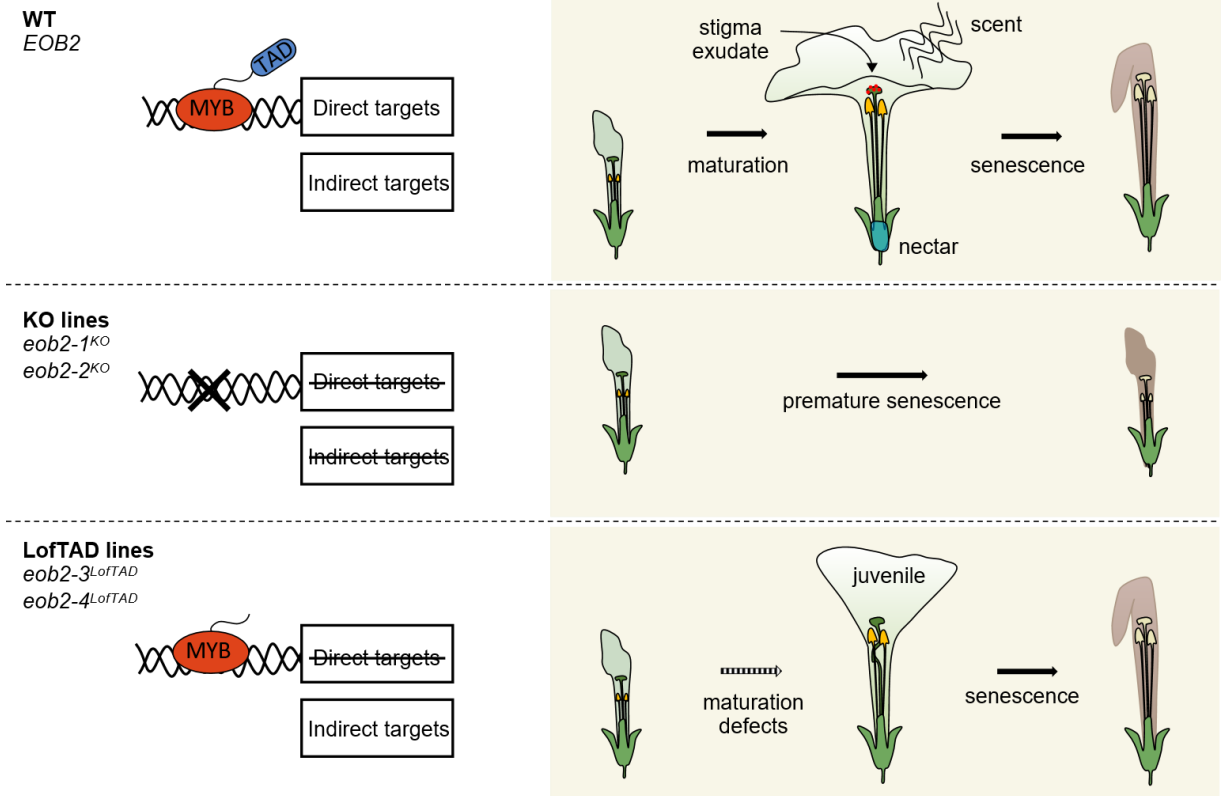


**Fig. 8 One gene, two mutations, contrasting phenotypes.**

Model to illustrate *EOB2* multi-functionality. The knockout (KO) lines and LofTAD lines do not present the same floral phenotype, while both lines are unable to activate target genes. This is the proof that *EOB2* is involved in other functions. Direct targets are most likely related to maturation-related genes like the secondary metabolism related genes, while indirect targets are probably senescence-related proteins/genes.

## New Phytologist Supporting Information

**Article title:** A single MYB transcription factor with multiple functions during flower development

**Authors:** Mathilde Chopy, Marta Binaghi, Gina Cannarozzi, Rayko Halitschke, Benoît Boachon, Roel Heutink, Dikki Pedenla Bomzan, Lea Jäggi, Geert van Geest, Julian C. Verdonk and Cris Kuhlemeier

**Article acceptance date:** 22-May-2023



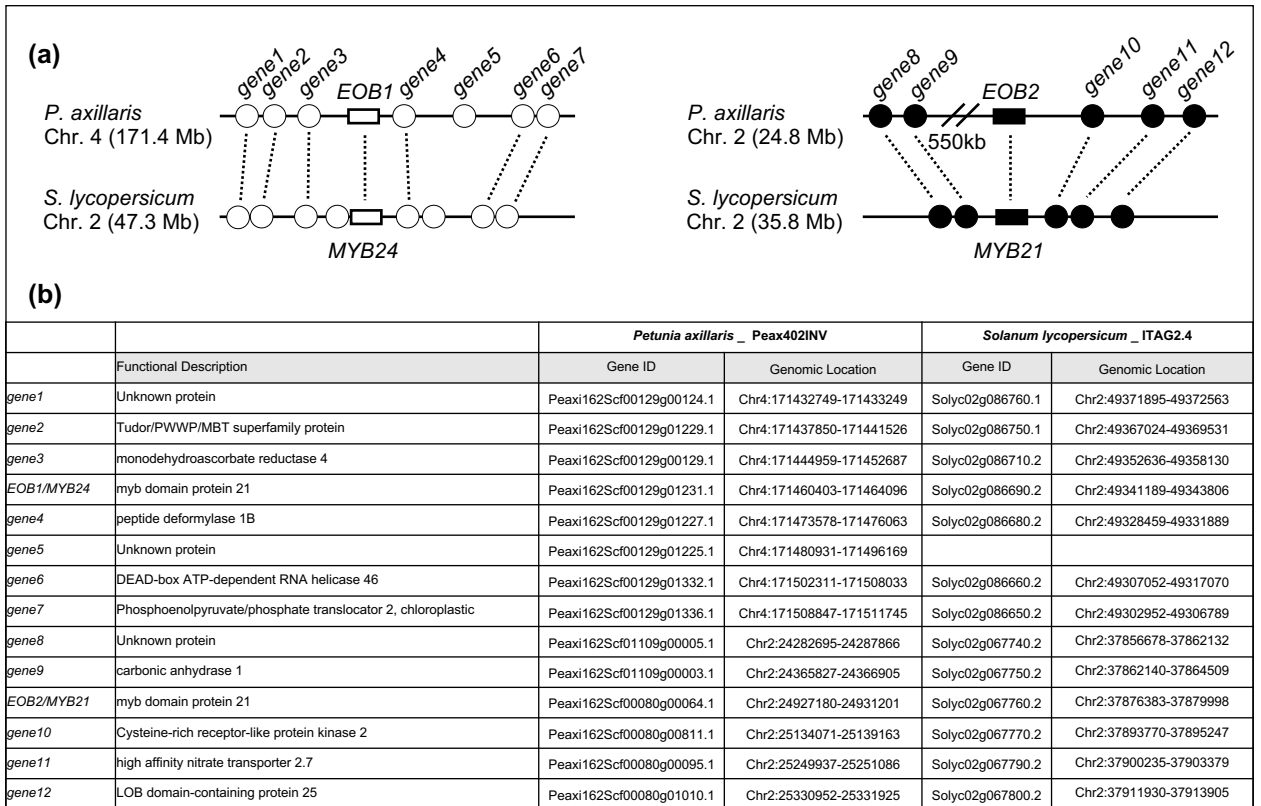


**Fig. S2** Microsynteny analysis comparing genomic regions surrounding *EOB1* or *EOB2* in *P. axillaris* and *S. lycopersicum*. **(a)** The microsynteny analysis was performed using GEvo from CoGe. The SG19 MYB's genomic locations are indicated in the left part. Rectangles indicate SG19 MYB genes, circles indicate the surrounding genes and lines indicate gene-poor regions. Syntenic genes are linked by dashed lines. Left: Genomic region surrounding *PaEOB1* (Peaxi162Scf00129g01231.1) compared with *SIMYB24* (Solyc02g086690.2). Right: Genomic region surrounding *PaEOB2* (Peaxi162Scf00080g00064.1) compared with *SIMYB21* (Solyc02g067760.2). No clear synteny was observed comparing *P. axillaris* and *A. thaliana*. Concerning *N. tabacum*, the genome assembly quality did not allow to perform the analysis. **(b)** Gene ID and coordinates of the genes used in the microsynteny analysis.

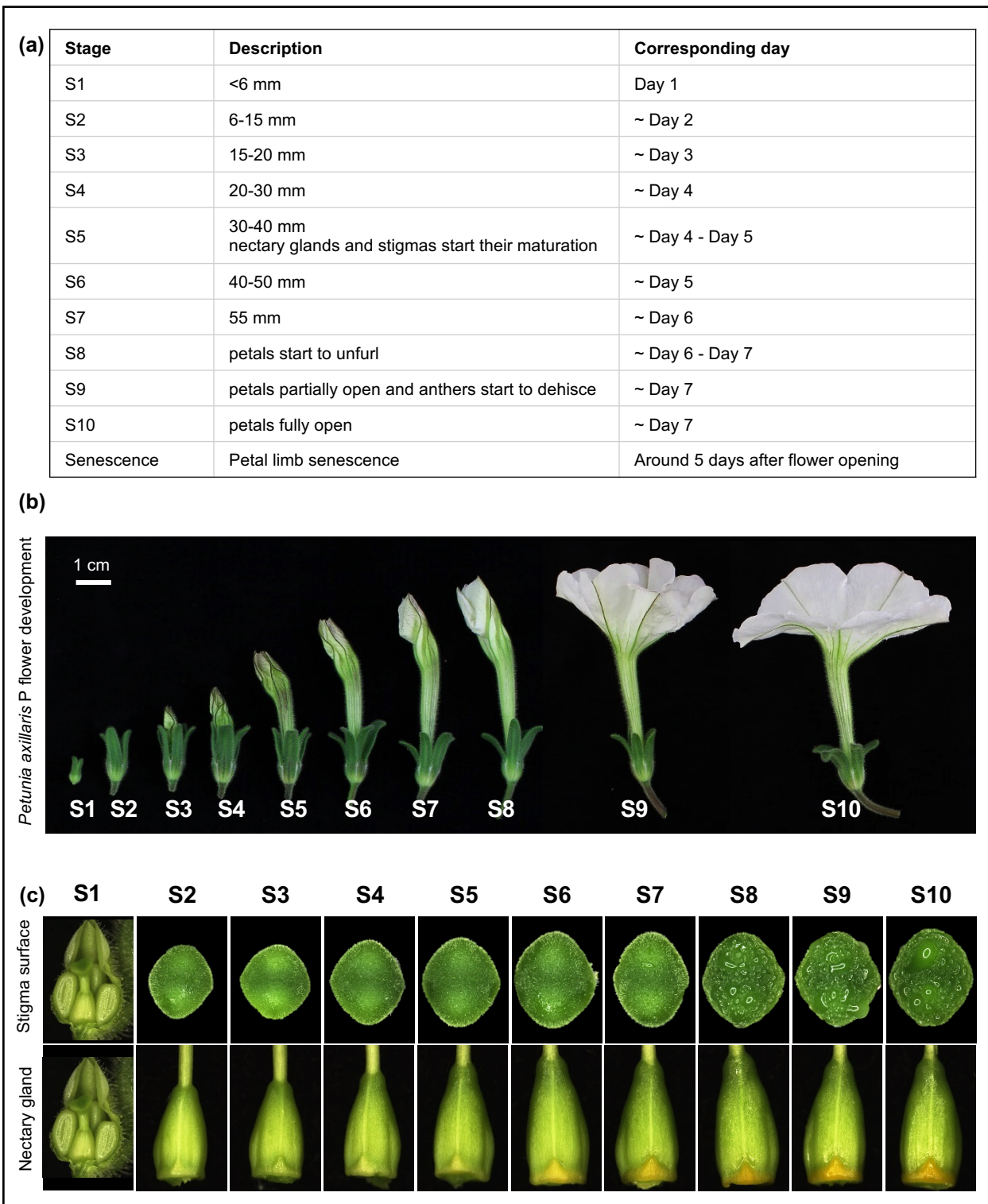


**Fig. S3** Description of the different *Petunia axillaris* P floral developmental stages used in this study.

**(a)** Table describing the different floral developmental stages used in this study over time, S1 to S10 = Stage 1 to Stage 10. **(b)** Pictures of the floral developmental stages of *P. axillaris* P. Scale bar = 1 cm. **(c)** Overview of the stigma surface and the nectary gland over the different developmental stages. The maturation phase of the stigma and nectary gland start at S5. The stigma secretes exudate after S5 and from S8 the stigma surface is covered by exudate droplets resulting in a wet stigma surface. The nectary gland starts to turn orange after S5 due to an accumulation of carotenoids and this process is accompanied by progressive nectar secretion, visible from S6 in the picture series. A metabolic switch may happen in nectary glands and stigma after stage 5.

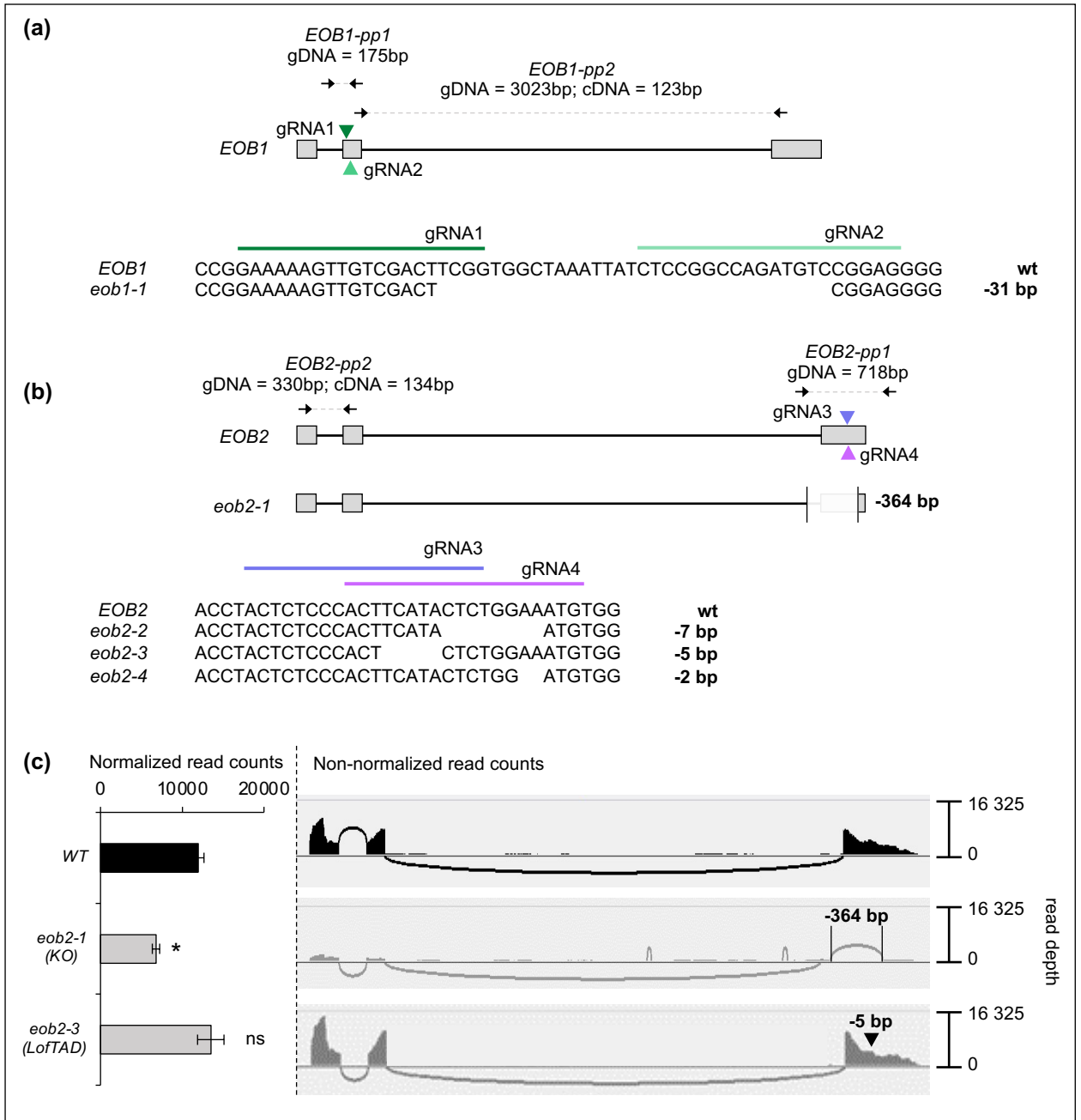


**Fig. S4** Construction of *eob1* and *eob2* mutant alleles by CRISPR-Cas9.

**(a)** *eob1-1* allele generated by CRISPR-Cas9. **(b)** *eob2-1* to 4 alleles generated by CRISPR-Cas9. Allele *eob2-1* consists of a 364bp deletion, leading to the removal of the last intron-exon junction affecting the normal splicing process. The primer pairs used for the genotyping (*EOB1-pp1* and *EOB2-pp1*) and RT-qPCR (*EOB1-pp2* and *EOB2-pp2*) are indicated. **(c)** Left: RNA sequencing analysis of *EOB2* expression in WT, *eob2-1* and *eob2-3* S5 petal limb (error bar = SD; significant differences \*,  $P < 0.05$ ; ns, non-significance; Student's t-test). Right: IGV software was used to construct Sashimi plots depicting splice junctions for the *EOB2* gene, from aligned RNA-seq data derived from S5 limb tissue. The library sizes (13 – 15 M for *eob2-1* and 25 – 60 M for WT) can explain the difference between the number of counts before and after normalization. But overall *EOB2* is lower compared to the WT.



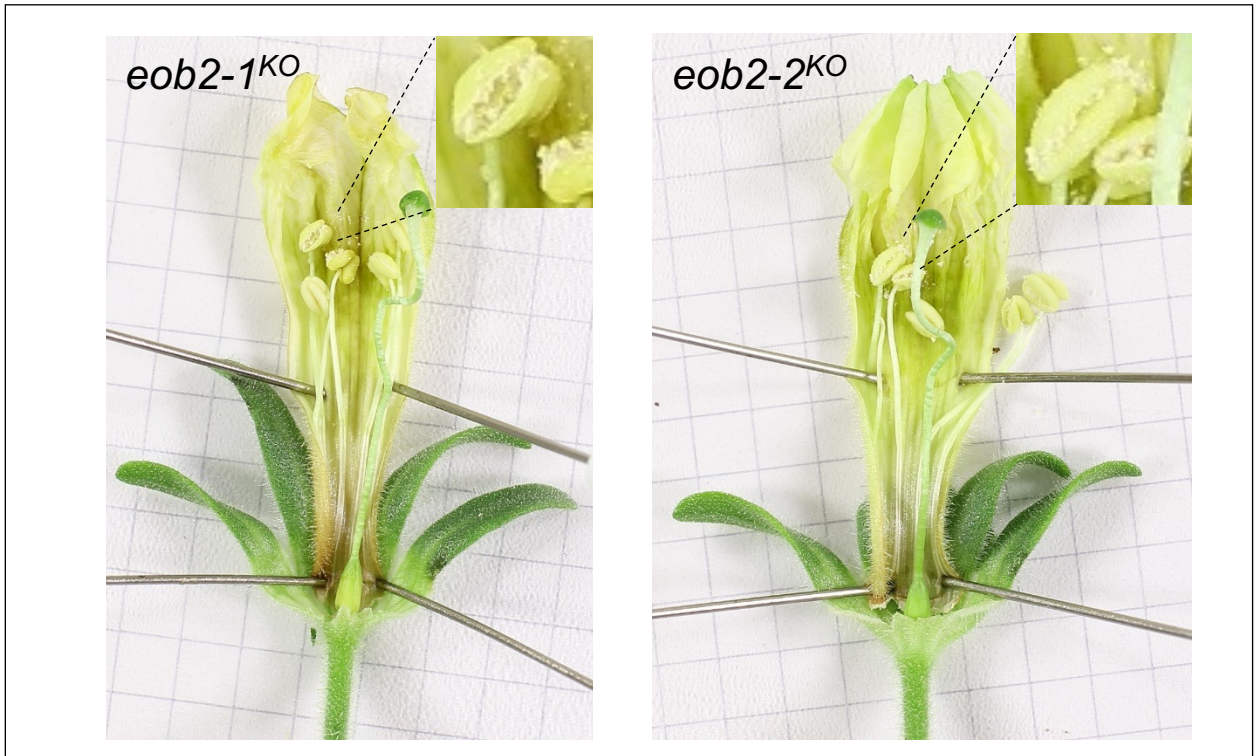


**Fig. S5** Observation of the internal floral organs of *eob2-1<sup>KO</sup>* and *eob2-2<sup>KO</sup>* flower buds. The dissected flower buds revealed that styles are twisted, nectary are not mature (yellow) and stamens can released fertile pollen several days after senescence.





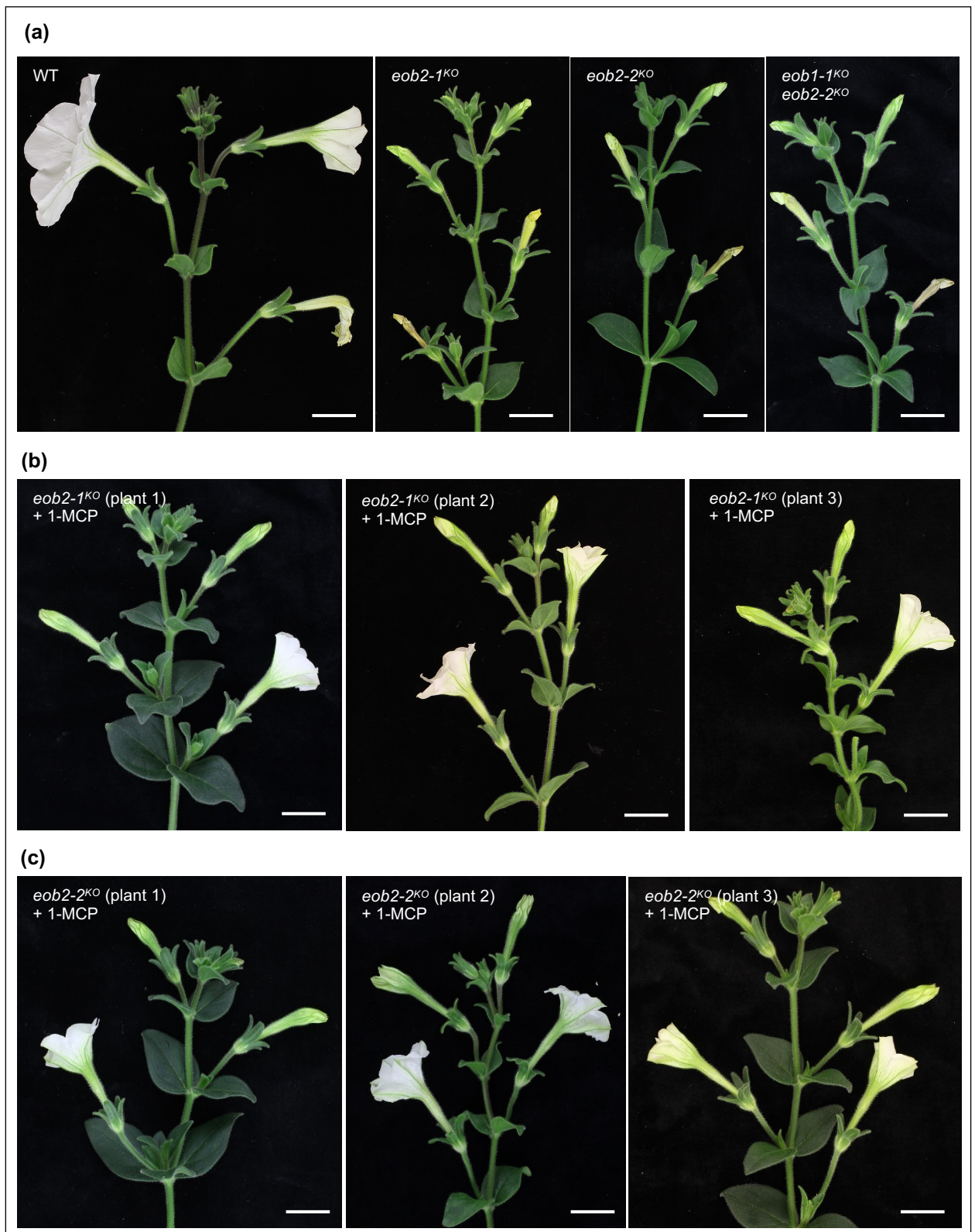
**Fig. S6** The *eob2-3<sup>LoFTAD</sup>* and *eob2-4<sup>LoFTAD</sup>* are semi-dominant alleles.

**(a)** Phenotype of the heterozygous mutant flowers. *eob2-3<sup>LoFTAD</sup>/+* or *eob2-4<sup>LoFTAD</sup>/+* displayed an intermediate phenotype between the WT and homozygous mutants. *eob2-1<sup>KO</sup>/+* or *eob2-2<sup>KO</sup>/+* resembled the WT. **(b)** Nectar measurements ( $n = 20$ ; error bar = SD). **(c)** Methylbenzoate measurements using a PTR-MS ( $n = 15$ ; error bar = SD).



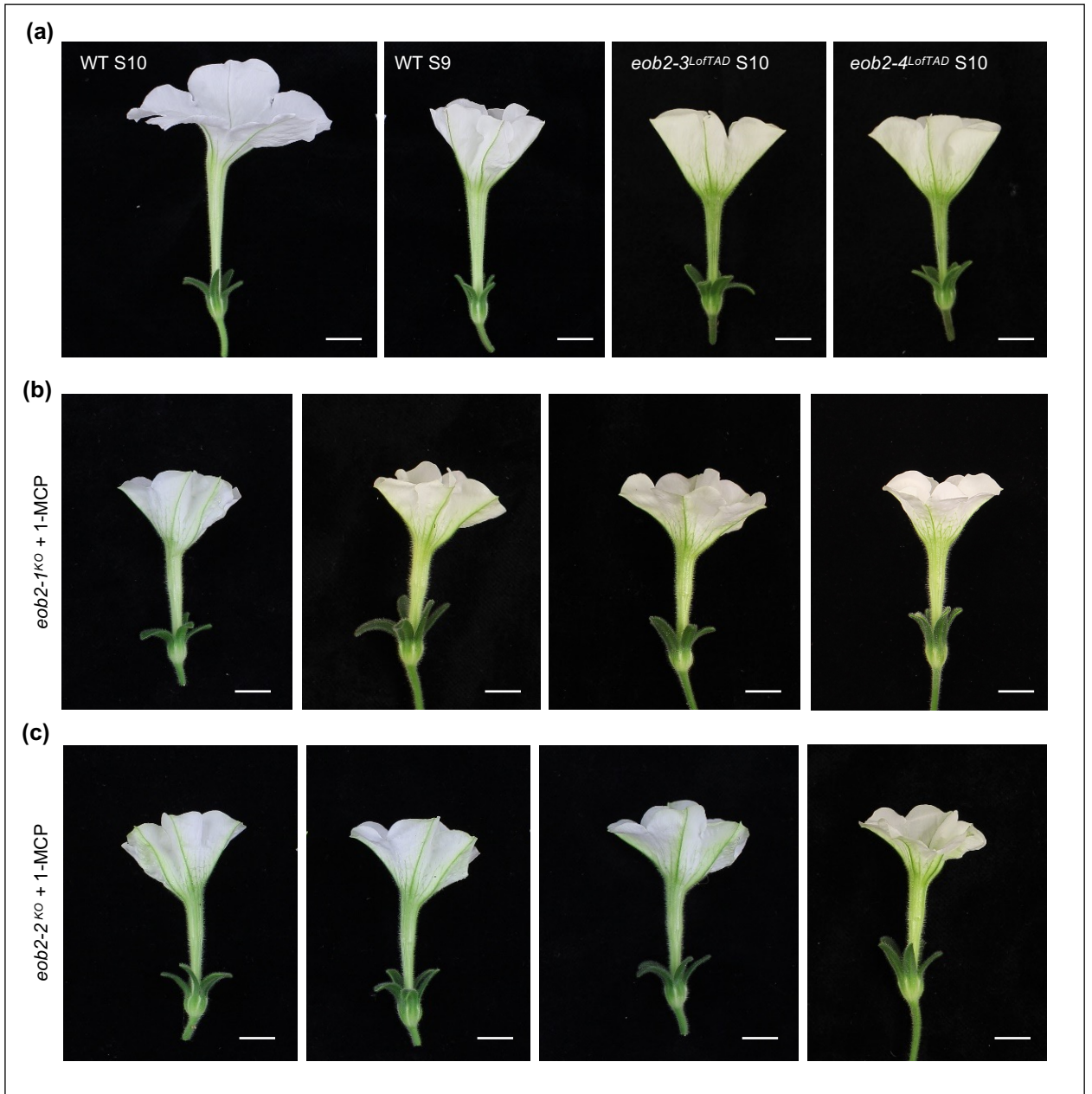


**Fig. S8** Additional phenotyping of *eob2-3<sup>LoTTAD</sup>*. Visible and UV pictures of WT and *eob2-3<sup>LoTTAD</sup>*. All flowers contain UV-absorbing pigments.



**Fig. S9** Branches of WT, *eob2-1<sup>KO</sup>* and *eob2-2<sup>KO</sup>* before and after 1-MCP treatment.



**(a)** Phenotypes of untreated WT, *eob2-1<sup>KO</sup>*, *eob2-2<sup>KO</sup>*, and the double mutant *eob1-1<sup>KO</sup> eob2-2<sup>KO</sup>* branches. **(b)** and **(c)** Partial rescue of the *eob2-1<sup>KO</sup>* **(b)** and *eob2-2<sup>KO</sup>* **(c)** phenotypes on 3 independent plant branches after 1-MCP treatment. Scale bars = 2cm.





**Fig. S10** *eob2-1<sup>KO</sup>* and *eob2-2<sup>KO</sup>* flowers after 1-MCP treatment, looked similar to *eob2-3<sup>LoTTAD</sup>* and *eob2-4<sup>LoTTAD</sup>*.  
**(a)** Phenotype of untreated WT, *eob2-3<sup>LoTTAD</sup>* and *eob2-4<sup>LoTTAD</sup>* flowers. **(b)** and **(c)** Partial rescue of the *eob2-1<sup>KO</sup>* **(b)** and *eob2-2<sup>KO</sup>* **(c)** phenotypes on 4 independent flowers after 1-MCP treatment. Scale bars = 1cm.



**(a) MA1037.1 (*AtMYB24*)**

	WT vs <i>eob2-3</i> limb S5	WT vs <i>eob2-3</i> nec S5	WT vs <i>eob2-3</i> limb S10	WT vs <i>eob2-3</i> nec S10	WT vs <i>eob2-3</i> common to the 4 conditions		WT vs <i>eob2-1</i> limb S5	
UP-regulated <i>eob2-3<sup>LoftAD</sup></i> >WT	<b>19.6%</b> 212 over 1084	<b>18.1%</b> 179 over 989	<b>21.1%</b> 686 over 3255	<b>19.2%</b> 485 over 2523	<b>18.3%</b> 22 over 120 ▲	UP-regulated <i>eob2-1<sup>KO</sup></i> >WT	<b>21%</b> 944 over 4485 +	
DOWN-regulated <i>eob2-3<sup>LoftAD</sup></i> <WT	<b>39.3%</b> 153 over 389	<b>35%</b> 292 over 834	<b>30.5%</b> 501 over 1645	<b>28.5%</b> 529 over 1854	<b>48.3%</b> 29 over 60 △	DOWN-regulated <i>eob2-1<sup>KO</sup></i> <WT	<b>27.4%</b> 867 over 3162 +	
common not DEGs padj>0.01; -1<log2FC<1	<b>22.9%</b> 1267 over 5522					△	not DEGs padj>0.01; -1<log2FC<1	<b>22.9%</b> 1393 over 6085 +
total in the <i>Pax</i> genome	<b>23%</b> 7517 over 32768					△	total in the <i>Pax</i> genome	<b>23%</b> 7517 over 32768 +

**(b) MA1408.1 (*FaEOB11*)**

	WT vs <i>eob2-3</i> limb S5	WT vs <i>eob2-3</i> nec S5	WT vs <i>eob2-3</i> limb S10	WT vs <i>eob2-3</i> nec S10	WT vs <i>eob2-3</i> common to the 4 conditions		WT vs <i>eob2-1</i> limb S5	
UP-regulated <i>eob2-3<sup>LoftAD</sup></i> >WT	<b>28.5%</b> 309 over 1084	<b>26.3%</b> 260 over 989	<b>30.9%</b> 1005 over 3255	<b>26.8%</b> 677 over 2523	<b>26.7%</b> 32 over 120 ●	UP-regulated <i>eob2-1<sup>KO</sup></i> >WT	<b>30.9%</b> 1387 over 4485 ◆	
DOWN-regulated <i>eob2-3<sup>LoftAD</sup></i> <WT	<b>40.6%</b> 158 over 389	<b>44.6%</b> 372 over 834	<b>39.4%</b> 648 over 1645	<b>39.6%</b> 734 over 1854	<b>53.3%</b> 32 over 60 ○	DOWN-regulated <i>eob2-1<sup>KO</sup></i> <WT	<b>36.7%</b> 1162 over 3162 ◆	
common not DEGs padj>0.01; -1<log2FC<1	<b>32%</b> 1767 over 5522					○	not DEGs padj>0.01; -1<log2FC<1	<b>32.3%</b> 1963 over 6085 ◆
total in the <i>Pax</i> genome	<b>31.9%</b> 10439 over 32768					○	total in the <i>Pax</i> genome	<b>31.9%</b> 10439 over 32768 ◆

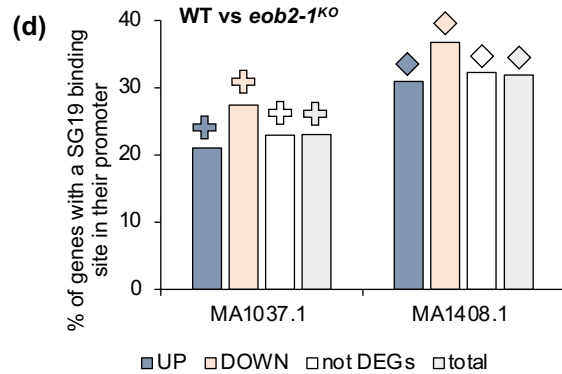
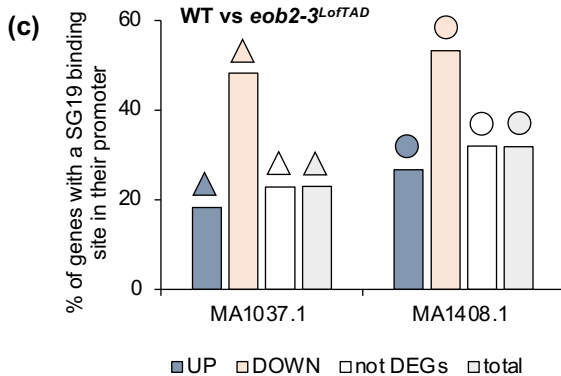


**Fig. S11** Percentage of genes with a 2kb promoter containing at least one putative R2R3-MYB SG19 binding site. The presence of a R2R3-MYB SG19 binding site in 2kb promoter was predicted using FIMO and two independent SG19 predicted motifs **(a)** MA1037.1 (*AtMYB24*) and **(b)** MA1408.1 (*FaEOB11*) ( $P < 1e-4$ ). The symbols indicate the percentage values used in **(c)** WT vs *eob2-3<sup>LoftAD</sup>* and **(d)** WT vs *eob2-1<sup>KO</sup>*.

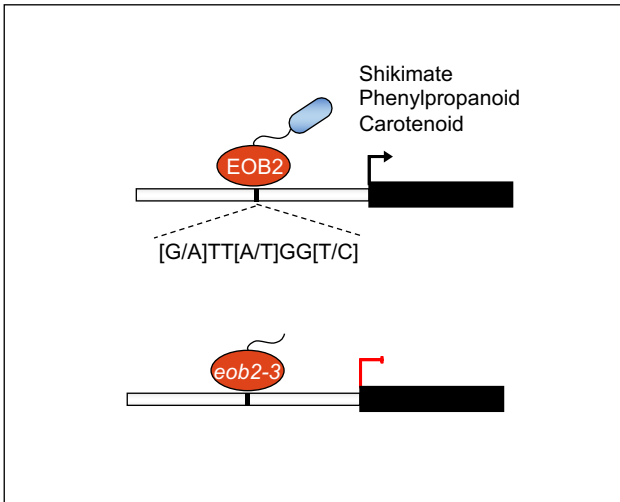


**Fig. S12** Model showing the direct activation of secondary metabolite related genes by EOB2. The promoter of secondary metabolite related genes is represented in white. The reduced expression of these genes in *eob2-3<sup>LoFTAD</sup>* limb and nectary tissues is most likely due to the missing TAD. Both EOB2 and *eob2-3<sup>LoFTAD</sup>* protein can bind the MYB-DNA-binding site ([G/A]TT[A/T]GG[T/C]) but only EOB2 can activate the transcription.

Organism	Protein-protein interactions	Methods	N- or C-terminus part interaction	Transcriptional function influence	Publication
<i>Arabidopsis thaliana</i>	JAZs* - AtMYB21 JAZs* - AtMYB24 AtMYB21 - AtMYB21 AtMYB24 - AtMYB24 AtMYB21 - AtMYB24	Y2H, LCI, BiFC	N-terminus	inhibition	Song <i>et al.</i> (2011)
	AtIlle bHLH - AtMYB21 AtIlle bHLH - AtMYB24	Y2H, Co-IP, BiFC	N-terminus	bHLH-MYB transcription complex	Qi <i>et al.</i> (2015)
	JAZs** - AtMYB21 JAZs** - AtMYB24 AtMYB24 - AtMYB21 AtMYB24 - AtMYB24	Y2H, LCI	N-terminus N- and C-terminus	inhibition	Huang <i>et al.</i> (2017)
	AtMYC2 - AtMYB21	Y2H, BiFC, <i>in vitro</i> pull-down	not tested	inhibition	Yang <i>et al.</i> (2020)
	DELLAs - AtMYB21 DELLAs - AtMYB24 AtJAZ1 - AtMYB21	Y2H, <i>in vitro</i> pull-down	N-terminus	inhibition	Huang <i>et al.</i> (2020)
	AtSnRK2.4 - AtMYB21	Y2H, <i>in vitro</i> pull-down, BiFC	N- and C-terminus	act together to mediate salt stress responses	Zhang <i>et al.</i> (2021)
<i>Petunia hybrida</i>	PhERF6 – EOB1	Y2H, BiFC, Co-IP	N-terminus	inhibition	Liu <i>et al.</i> (2017)
<i>Solanum lycopersicum</i>	SIJAZ9 – SIMYB21	Y2H, BiFC, splitTALE	not tested	not tested	Schubert <i>et al.</i> (2019)
<i>Freesia hybrida</i>	FhMYC2 - FhMYB21L2	Y2H, BiFC,	not tested	inhibition	Yang <i>et al.</i> (2020)
<i>Hedychium coronarium</i>	HcMYB1 - HcIAA4	Y2H, BiFC	not tested	inhibition	Ke <i>et al.</i> (2021)

**Table S1** Summary of protein-protein interactions involving members of the R2R3-MYB SG19 reported in the literature. List of abbreviations: Bimolecular Fluorescence Complementation (BiFC), Yeast-two-Hybrid (Y2H), Co-Immunoprecipitation (Co-IP), Luciferase Complementation Imaging (LCI), Jasmonate zim-domain (JAZ), Ethylene Response Factor (ERF), repressors of gibberellin (DELLAs), Sucrose non-fermenting-1-related protein kinase 2 (salt tolerance, SnRK2). JAZs\* = JAZ1, JAZ8, JAZ11, JAZs\*\* = JAZ1, JAZ2, JAZ3, JAZ4, JAZ5, JAZ6, JAZ8, JAZ10, JAZ11, JAZ12, DELLAs = AtRGA, AtGAI, AtRGL1, AtRGL2, AtRGL3 and Ille bHLH = bHLH TFs of the Ille clade such as MYC2, MYC3, MYC4, MYC5.



Organism	Direct target gene	Methods	Publication
<i>Arabidopsis thaliana</i>	AtMYB21 → <i>PAL1</i> , <i>PAL2</i> AtMYB21 → <i>UGT73B2</i> AtMYB21 → <i>UGT79B6</i> AtMYB21 → <i>AtMYB24</i> AtMYB24 → <i>AtMYB21</i>	DL	Battat <i>et al.</i> (2019)
	AtMYB21 → <i>AtTPS14</i> AtMYB21 → <i>AtTPS21</i>	transient protoplast, EMSA	Yang <i>et al.</i> (2020)
	AtMYB21 → <i>AtFLS1</i>	Y1H, DL, ChIP, EMSA	Zhang <i>et al.</i> (2021)
<i>Nicotiana tabacum</i> <i>Antirrhinum majus</i>	MYB305 → <i>PAL2</i> MYB305 → <i>CHS</i>	Transactivation, EMSA	Sablowski <i>et al.</i> (1994) Moyano <i>et al.</i> (1996)
<i>Nicotiana tabacum</i>	MYB305 → <i>NEC1</i> MYB305 → <i>NEC5</i>	EMSA	Liu <i>et al.</i> (2009)
	MYB305 → <i>AGP</i>	indirect	Liu <i>et al.</i> (2012)
	NtMYB305a → <i>NtPMT1a</i>	Y1H, ChIP, EMSA	Bian <i>et al.</i> (2021)
<i>Petunia hybrida</i>	PhEOB2 → <i>PhPAL</i> PhEOB2 → <i>PhIGS</i>	Transient protoplast transfection	Spitzer-Rimon <i>et al.</i> (2010)
	PhEOB2 → <i>PhODO1</i>	Transactivation, EMSA	Moerkercke <i>et al.</i> (2011)
	PhEOB2 → <i>PhEOB1</i> PhEOB1 → <i>PhPAL</i> PhEOB1 → <i>PhIGS</i> PhEOB1 → <i>PhODO1</i>	Transient protoplast transfection, EMSA, Y1H,	Spitzer-Rimon <i>et al.</i> (2012)
<i>Freesia vesca</i>	FaEOB2 → <i>FvCAD1</i> FaEOB2 → <i>PhODO1</i>	Transactivation	Medina-Puche <i>et al.</i> (2015)
<i>Freesia hybrida</i>	FhMYB21L2 → <i>FhTPS1</i>	Transient protoplast transfection, ChIP, EMSA	Yang <i>et al.</i> (2020)
<i>Malus domestica</i>	MYB305 → <i>Machi3-1</i>	Expression correlation analysis	Kurilla <i>et al.</i> (2019)
<i>Lilium longiflorum</i>	LIMYB305 → <i>LIHSC70</i>	Y1H, DL	Wu <i>et al.</i> (2021)
<i>Hedychium coronarium</i>	HcMYB2 → <i>HcBSMT2</i> HcMYB1 → <i>HcBSMT2</i> HcMYB1 → <i>HcTPS5</i>	Y1H, DL	Ke <i>et al.</i> (2021)
<i>Vitis vinifera</i>	VvMYB24 → 20 terpene related genes ( <i>VvTPS35</i> ) VvMYB24 → 6 carotenoid related genes ( <i>GGPS1</i> , <i>CRTISO2</i> , <i>LCYE</i> ) VvMYB24 → 30 photosynthesis and light-response genes <i>VvHYH</i>	DAP-seq, DL	Zhang <i>et al.</i> (2021) (PREPRINT)
<i>Chrysanthemum morifolium</i>	CmMYB21 →  <i>CmDFR</i>	Y1H, DL	Wang <i>et al.</i> (2022)

**Table S2** Summary of the direct target genes of members of the R2R3-MYB SG19 reported in the literature. R2R3-MYB SG19 are prominently activators, with one exception identified in *Chrysanthemum morifolium*. List of abbreviations: Chromatin ImmunoPrecipitation (ChIP), Electrophoretic Mobility Shift Assay (EMSA), Yeast one-Hybrid (Y1H), Dual-Luciferase (DL), DNA Affinity Purification sequencing (DAP-seq). Shikimate/Phenylpropanoids/Benzaldehyde: Emission Of Benzenoids (EOB), Phenylalanine Ammonia-Lyase (PAL), Chalcone Synthase (CHS), Isoeugenol Synthase (IGS), Cinnamyl Alcohol Dehydrogenase (CAD), Odorant 1 (ODO1). Nectary related: ADP-glucose pyrophosphorylase (small subunit, AGPs), Chitinase (Machi). Terpene related: Terpene synthase (TPS). Flavonoid related: Dihydroflavonol 4-Reductase (DFR), UDP-Glucuronosyltransferase (UGT), Flavonol Synthase (FLS). Carotenoid related: Geranylgeranyl Diphosphate Synthase 1 (GGPS1), Carotenoid Isomerase (CRTISO2), Lycopene Epsilon Cyclase (LCYE). Photosynthesis and light-response genes: HY5 Homolog (HYH). Nicotine related: Putrescine *N*-Methyltransferase (PMT). Others: Heat Shock protein (HSC).

Target gene	gRNA#	gRNA sequence (from 5'-3')
<i>EOB1</i> _ Peaxi162Scf00129g01231.1	gRNA1	GAAAAAGTTGTCGACTTCGG
<i>EOB1</i> _ Peaxi162Scf00129g01231.1	gRNA2	CTCCGGCCAGATGTCCGGAG
<i>EOB2</i> _ Peaxi162Scf00080g00064.1	gRNA3	TACTCTCCCCTTCATACTC
<i>EOB2</i> _ Peaxi162Scf00080g00064.1	gRNA4	CACTTCATACTCTGGAAATG

**Table S3** gRNA sequences used to target *EOB1* and *EOB2*.

Target gene	Application	Primer pair	Forward primer (from 5'-3')	Reverse primer (from 5'-3')
<i>EOB1</i> _ Peaxi162Scf00129g01231.1	Genotyping	EOB1-pp1	CGACAACCTATTTGAGATTGAGACG	CACTTAGCATGCAGTTCATAATC
<i>EOB2</i> _ Peaxi162Scf00080g00064.1	Genotyping	EOB2-pp1	CAAATACATGGTGTACAGGGC	TAACCATAGGCACCTCCATG
<i>EOB1</i> _ Peaxi162Scf00129g01231.1	RT-qPCR	EOB1-pp2	CAGCTCTTGATTATGGAAGTGC	GTGCTTCTGTATCTAGTCTC
<i>EOB2</i> _ Peaxi162Scf00080g00064.1	RT-qPCR	EOB2-pp2	GAGGAAAGGACCTTGACTATG	ACCGAAGCCGACAACCTT
<i>ODO1</i> _ Peaxi162Scf00002g00037.1	RT-qPCR	ODO1-pp1	TGCTTCAACCATGTGGAATTG	TCCGTGCCTGTTCTCTACGTT
<i>TPS1</i> _ Peaxi162Scf00074g00143.1	RT-qPCR	TPS1-pp1	GCAACTGAAGCGCCTATGTT	TGTGTATCCATCCGCCTCTT
<i>RAN1</i> _ Peaxi162Scf01372g00049.1	RT-qPCR	RAN1-pp1	AAGCTCCCACCTGTCTGAAAA	AACAGATTGCCGAAGCCA
<i>ACTIN11</i> _ Peaxi162Scf00258g00618.1	RT-qPCR	ACT11-pp1	TGCACTCCCACATGCTATCCT	TCAGCCGAAGTGGTGAAGAG
<i>EOB1</i> _ Peaxi162Scf00129g01231.1	RT-qPCR for transient	EOB1-pp3	TGTGAGCACATGATCAACAAG	TCCAGTGATGAAGATGGAGAATAG
<i>EOB2</i> _ Peaxi162Scf00080g00064.1	RT-qPCR for transient	EOB2-pp3	GCCAAATGTCTAATGGTCCAAAT	TTAGGGCCTGCTTGAAAAAG
<i>CAS9</i> _ pHSE401 vector	Genotyping	CAS9-pp1	CTGCAGAATGAGAAGCTCTAC	GACGATATTCACCTGTGGCATG
<i>EOB1</i> _ Peaxi162Scf00129g01231.1	Cloning	EOB1-pp4	<b>GGGGACAAGTTTGTACAAAAAAGCAGGCTT</b> CATGGATAAAAAGAACATGCAATTCTC	<b>GGGGACCACCTTTGTACAAGAAAGCTGGGTC</b> TTAGTTGGTTGCATCATTAAAGC
<i>EOB2</i> _ Peaxi162Scf00080g00064.1	Cloning	EOB2-pp4	<b>GGGGACAAGTTTGTACAAAAAAGCAGGCTT</b> CATGGATAAAAACCATGCAACTCTC	<b>GGGGACCACCTTTGTACAAGAAAGCTGGGTC</b> TTAATCACCATTAAAGCAATTGCATG
<i>eob2-2</i> _ Peaxi162Scf00080g00064.1	Cloning	eob2-2-pp1	<b>GGGGACAAGTTTGTACAAAAAAGCAGGCTT</b> CATGGATAAAAACCATGCAACTCTC	<b>GGGGACCACCTTTGTACAAGAAAGCTGGGTC</b> CTAGCTAACTAGAGGCTTAACCTTTTGG
<i>eob2-3</i> _ Peaxi162Scf00080g00064.1	Cloning	eob2-3-pp1	<b>GGGGACAAGTTTGTACAAAAAAGCAGGCTT</b> CATGGATAAAAACCATGCAACTCTC	<b>GGGGACCACCTTTGTACAAGAAAGCTGGGTC</b> TTAGGGCTGCTTGAAAAAGT

**Table S4** Sequence description of primers used for this work.  
**Boldface:** recombination site for cloning

<b>Samples</b>	<b>Genotype</b>	<b>Stage</b>	<b>Tissue</b>
Sample 1	<i>eob2-1</i>	S5 (flower bud of ~3.5 cm, just before dark)	3 limbs
Sample 2	<i>eob2-1</i>	S5 (flower bud of ~3.5 cm, just before dark)	3 limbs
Sample 3	<i>eob2-1</i>	S5 (flower bud of ~3.5 cm, just before dark)	3 limbs
Sample 4	<i>eob2-3</i>	S5 (flower bud of ~3.5 cm, just before dark)	3 limbs
Sample 5	<i>eob2-3</i>	S5 (flower bud of ~3.5 cm, just before dark)	3 limbs
Sample 6	<i>eob2-3</i>	S5 (flower bud of ~3.5 cm, just before dark)	3 limbs
Sample 7	PaxP WT	S5 (flower bud of ~3.5 cm, just before dark)	3 limbs
Sample 8	PaxP WT	S5 (flower bud of ~3.5 cm, just before dark)	3 limbs
Sample 9	PaxP WT	S5 (flower bud of ~3.5 cm, just before dark)	3 limbs
Sample 10	<i>eob2-3</i>	S7 (flower bud of ~5.5 cm, just before dark)	2 limbs
Sample 11	<i>eob2-3</i>	S7 (flower bud of ~5.5 cm, just before dark)	2 limbs
Sample 12	<i>eob2-3</i>	S7 (flower bud of ~5.5 cm, just before dark)	2 limbs
Sample 13	PaxP WT	S7 (flower bud of ~5.5 cm, just before dark)	2 limbs
Sample 14	PaxP WT	S7 (flower bud of ~5.5 cm, just before dark)	2 limbs
Sample 15	PaxP WT	S7 (flower bud of ~5.5 cm, just before dark)	2 limbs
Sample 16	<i>eob2-3</i>	S10 (open flower; 1 DPA, just before dark)	1 limb
Sample 17	<i>eob2-3</i>	S10 (open flower; 1 DPA, just before dark)	1 limb
Sample 18	<i>eob2-3</i>	S10 (open flower; 1 DPA, just before dark)	1 limb
Sample 19	PaxP WT	S10 (open flower; 1 DPA, just before dark)	1 limb
Sample 20	PaxP WT	S10 (open flower; 1 DPA, just before dark)	1 limb
Sample 21	PaxP WT	S10 (open flower; 1 DPA, just before dark)	1 limb
Sample 25	<i>eob2-3</i>	S5 (flower bud of ~3.5 cm, just before dark)	5 basal ovaries
Sample 26	<i>eob2-3</i>	S5 (flower bud of ~3.5 cm, just before dark)	5 basal ovaries
Sample 27	<i>eob2-3</i>	S5 (flower bud of ~3.5 cm, just before dark)	5 basal ovaries
Sample 28	PaxP WT	S5 (flower bud of ~3.5 cm, just before dark)	5 basal ovaries
Sample 29	PaxP WT	S5 (flower bud of ~3.5 cm, just before dark)	5 basal ovaries
Sample 30	PaxP WT	S5 (flower bud of ~3.5 cm, just before dark)	5 basal ovaries
Sample 31	<i>eob2-3</i>	S10 (open flower; 1 DPA, just before dark)	5 basal ovaries
Sample 32	<i>eob2-3</i>	S10 (open flower; 1 DPA, just before dark)	5 basal ovaries
Sample 33	<i>eob2-3</i>	S10 (open flower; 1 DPA, just before dark)	5 basal ovaries
Sample 34	PaxP WT	S10 (open flower; 1 DPA, just before dark)	5 basal ovaries
Sample 35	PaxP WT	S10 (open flower; 1 DPA, just before dark)	5 basal ovaries
Sample 36	PaxP WT	S10 (open flower; 1 DPA, just before dark)	5 basal ovaries

**Table S5** Description of the samples collected for the RNA sequencing experiment. Day post anthesis (DPA)

Genotype	Stage	Tissues	Starch	Carotenoids
<i>eob2-3</i>	S5 (flower bud of ~3.5 cm, just before dark)	5 limbs	yes	no
<i>eob2-3</i>	S5 (flower bud of ~3.5 cm, just before dark)	5 limbs	yes	no
<i>eob2-3</i>	S5 (flower bud of ~3.5 cm, just before dark)	5 limbs	yes	no
<i>eob2-3</i>	S10 (open flower; 1 DPA, just before dark)	3 limbs	yes	no
<i>eob2-3</i>	S10 (open flower; 1 DPA, just before dark)	3 limbs	yes	no
<i>eob2-3</i>	S10 (open flower; 1 DPA, just before dark)	3 limbs	yes	no
PaxP WT	S5 (flower bud of ~3.5 cm, just before dark)	5 limbs	yes	no
PaxP WT	S5 (flower bud of ~3.5 cm, just before dark)	5 limbs	yes	no
PaxP WT	S5 (flower bud of ~3.5 cm, just before dark)	5 limbs	yes	no
PaxP WT	S10 (open flower; 1 DPA, just before dark)	3 limbs	yes	no
PaxP WT	S10 (open flower; 1 DPA, just before dark)	3 limbs	yes	no
PaxP WT	S10 (open flower; 1 DPA, just before dark)	3 limbs	yes	no
<i>eob2-3</i>	S5 (flower bud of ~3.5 cm, just before dark)	~67 basal ovaries	yes	no
<i>eob2-3</i>	S5 (flower bud of ~3.5 cm, just before dark)	~67 basal ovaries	yes	no
<i>eob2-3</i>	S5 (flower bud of ~3.5 cm, just before dark)	~67 basal ovaries	yes	no
<i>eob2-3</i>	S10 (open flower; 1 DPA, just before dark)	~55 basal ovaries	yes	yes
<i>eob2-3</i>	S10 (open flower; 1 DPA, just before dark)	~55 basal ovaries	yes	yes
<i>eob2-3</i>	S10 (open flower; 1 DPA, just before dark)	~55 basal ovaries	yes	yes
PaxP WT	S5 (flower bud of ~3.5 cm, just before dark)	~40 basal ovaries	yes	no
PaxP WT	S5 (flower bud of ~3.5 cm, just before dark)	~40 basal ovaries	yes	no
PaxP WT	S5 (flower bud of ~3.5 cm, just before dark)	~40 basal ovaries	yes	no
PaxP WT	S10 (open flower; 1 DPA, just before dark)	~45 basal ovaries	yes	yes
PaxP WT	S10 (open flower; 1 DPA, just before dark)	~45 basal ovaries	yes	yes
PaxP WT	S10 (open flower; 1 DPA, just before dark)	~45 basal ovaries	yes	yes

**Table S6** Description of the samples collected for the starch and carotenoid measurements. Day post anthesis (DPA). yes and no indicate which compounds were measured.

Alleles	T0 plants	x		T1 plant selected	x		Final homozygous mutant lines	
<i>eob1-1</i> (-31bp)	PaxP background <i>eob1-1/EOB1</i> CAS9 positive	x	PaxP wild-type	PaxP background <i>eob1-1/EOB1</i> CAS9 negative	x	Self	PaxP background <i>eob1-1/eob1-1</i> CAS9 negative	
<i>eob2-1</i> (-364bp)	PaxP background <i>eob2-1/EOB2</i> CAS9 positive	x	PaxP wild-type	PaxP background <i>eob2-1/EOB2</i> CAS9 negative	x	Self	PaxP background <i>eob2-1/eob2-1</i> CAS9 negative	maintained by cuttings
<i>eob2-2</i> (-7bp)	PaxP background <i>eob2-2/eob2-4</i> CAS9 positive	x	PaxP wild-type	PaxP background <i>eob2-2/EOB2</i> CAS9 negative	x	Self	PaxP background <i>eob2-2/eob2-2</i> CAS9 negative	maintained by cuttings
<i>eob2-3</i> (-5bp)	PaxP background <i>eob2-3/EOB2</i> CAS9 positive	x	PaxP wild-type	PaxP background <i>eob2-3/EOB2</i> CAS9 negative	x	Self	PaxP background <i>eob2-3/eob2-3</i> CAS9 negative	
<i>eob2-4</i> (-2bp)	PaxP background <i>eob2-2/eob2-4</i> CAS9 positive	x	PaxP wild-type	PaxP background <i>eob2-4/EOB2</i> CAS9 negative	x	Self	PaxP background <i>eob2-4/eob2-4</i> CAS9 negative	
<i>eob1-1</i> (-31bp) <i>eob2-2</i> (-7bp)	PaxP background <i>eob1-1/EOB1</i> CAS9 positive	x	PaxP background <i>eob2-2/eob2-4</i> CAS9 positive	PaxP background <i>eob1-1/EOB1</i> <i>eob2-2/EOB2</i> CAS9 negative	x	Self	PaxP background <i>eob1-1/eob1-1</i> <i>eob2-2/eob2-2</i> CAS9 negative	maintained by cuttings

**Table S7** From the T0 transgenic lines obtained by CRISPR-Cas9 to the final homozygous mutant lines used in this study.

comparison	motif	regulation	with_ regulated	without_ regulated	with	without	fraction	expected_ fraction	p_value	p_adjusted	log10_ padj	fraction_diff
WT vs eob2-3 _limb S5	MA1408.1	up	309	775	10439	22329	0.285055351	0.318572998	0.016958118	0.020349742	1.69	-0.033517647
WT vs eob2-3 _nec S5	MA1408.1	up	260	729	10439	22329	0.26289181	0.318572998	0.000117851	0.000217572	3.66	-0.055681188
WT vs eob2-3 _limb S10	MA1408.1	up	1005	2250	10439	22329	0.30875576	0.318572998	0.211787372	0.23104077	0.64	-0.009817238
WT vs eob2-3 _nec S10	MA1408.1	up	677	1846	10439	22329	0.268331352	0.318572998	1.20842E-08	2.90021E-08	7.54	-0.050241646
common to the 4 conditions	MA1408.1	up	32	88	10439	22329	0.266666667	0.318572998	0.239775753	0.250200785	0.6	-0.051906331
WT vs eob2-1 _limb S5	MA1408.1	up	1387	3098	10439	22329	0.309253066	0.318572998	0.15226853	0.174021177	0.76	-0.009319932
WT vs eob2-3 _limb S5	MA1408.1	down	158	231	10439	22329	0.406169666	0.318572998	0.000290813	0.0004653	3.33	0.087596668
WT vs eob2-3 _nec S5	MA1408.1	down	372	462	10439	22329	0.46043165	0.318572998	8.07268E-15	9.68722E-14	13.01	0.127470167
WT vs eob2-3 _limb S10	MA1408.1	down	648	997	10439	22329	0.393920973	0.318572998	3.80814E-11	1.52325E-10	9.82	0.075347975
WT vs eob2-3 _nec S10	MA1408.1	down	734	1120	10439	22329	0.395900755	0.318572998	4.95218E-13	2.64087E-12	11.58	0.077327757
common to the 4 conditions	MA1408.1	down	32	28	10439	22329	0.533333333	0.318572998	0.000711522	0.001067283	2.97	0.214760335
WT vs eob2-1 _limb S5	MA1408.1	down	1162	2000	10439	22329	0.367488931	0.318572998	8.82443E-10	2.64733E-09	8.58	0.048915933
comparison	motif	regulation	with_ regulated	without_ regulated	with	without	fraction	expected_ fraction	p_value	p_adjusted	log10_ padj	fraction_diff
WT vs eob2-3 _limb S5	MA1037.1	up	212	872	7517	25251	0.195571956	0.229400635	0.006554535	0.00873938	2.06	-0.033828679
WT vs eob2-3 _nec S5	MA1037.1	up	179	810	7517	25251	0.1809909	0.229400635	0.00019159	0.000328441	3.48	-0.048409735
WT vs eob2-3 _limb S10	MA1037.1	up	686	2569	7517	25251	0.210752688	0.229400635	0.007373347	0.009313701	2.03	-0.018647947
WT vs eob2-3 _nec S10	MA1037.1	up	485	2038	7517	25251	0.19223147	0.229400635	2.78724E-06	6.08124E-06	5.22	-0.037169164
common to the 4 conditions	MA1037.1	up	22	98	7517	25251	0.183333333	0.229400635	0.276273132	0.276273132	0.56	-0.046067301
WT vs eob2-1 _limb S5	MA1037.1	up	944	3541	7517	25251	0.210479376	0.229400635	0.001154161	0.001629404	2.79	-0.018921259
WT vs eob2-3 _limb S5	MA1037.1	down	153	236	7517	25251	0.393316195	0.229400635	3.77189E-13	2.64087E-12	11.58	0.163915561
WT vs eob2-3 _nec S5	MA1037.1	down	292	542	7517	25251	0.350119904	0.229400635	1.34272E-15	3.22252E-14	13.49	0.120719269
WT vs eob2-3 _limb S10	MA1037.1	down	501	1144	7517	25251	0.304559271	0.229400635	5.50182E-13	2.64087E-12	11.58	0.075158636
WT vs eob2-3 _nec S10	MA1037.1	down	529	1325	7517	25251	0.285329018	0.229400635	8.71986E-09	2.32529E-08	7.63	0.055928384
common to the 4 conditions	MA1037.1	down	29	31	7517	25251	0.483333333	0.229400635	1.72634E-05	3.45268E-05	4.46	0.253932699
WT vs eob2-1 _limb S5	MA1037.1	down	867	2295	7517	25251	0.274193548	0.229400635	5.96085E-10	2.04372E-09	8.69	0.044792914

**Table S8** Fraction of genes with a 2kb promoter containing at least one putative R2R3-MYB SG19 binding site.

The presence of a R2R3-MYB SG19 binding site in 2kb promoter was predicted using FIMO and two independent SG19 predicted motifs MA1408.1 (*FaEOB1*) and MA1037.1 (*AtMYB24*) ( $P < 1e-4$ ). “with-regulated” is for up or down regulated genes with a motif in the promoter and “with” is for the total number of genes identified in *Petunia* (32,768) with a motif in the promoter.

	<b>Gene ID _ Figure 5C</b>
ACS #1	Peaxi162Scf00074g01725.1
ACS #2	Peaxi162Scf00620g00121.1
ACS #3	Peaxi162Scf00102g01634.1
ACS #4	Peaxi162Scf00381g00219.1
ACS #5	Peaxi162Scf00192g00920.1
ACS #6	Peaxi162Scf00102g01343.1
ACS #7	Peaxi162Scf00096g01846.1
ACS #8	Peaxi162Scf00822g00212.1
	<b>Gene ID _ Figure 5C</b>
ACO #1	Peaxi162Scf00521g00613.1
ACO #2	Peaxi162Scf00294g00812.1
ACO #3	Peaxi162Scf01096g00025.1
ACO #4	Peaxi162Scf00047g01927.1
ACO #5	Peaxi162Scf01333g00015.1
ACO #6	Peaxi162Scf01333g00016.1
	<b>Gene ID _ Figure 6C</b>
EOB1	Peaxi162Scf00129g01231.1
CM1	Peaxi162Scf00166g00931.1
BSMT1	Peaxi162Scf00047g01123.1
BSMT2	Peaxi162Scf00047g00116.1
EGS	Peaxi162Scf00020g01714.1
IGS1	Peaxi162Scf00889g00229.1
IGS3	Peaxi162Scf00185g01622.1
Z-ISO	Peaxi162Scf00378g00631.1
ZDS	Peaxi162Scf00404g00021.1
LCY B	Peaxi162Scf00091g00064.1
CCD	Peaxi162Scf00953g00316.1
	<b>Gene ID _ Figure 7B</b>
BAM	Peaxi162Scf00715g00216.1

**Table S9** Gene ID of genes used in this study.

Gene IDs of the eight *1-Aminocyclopropane-1-Carboxylic Acid Synthase (ACS)* genes and six *1-Aminocyclopropane-1-Carboxylic Acid Oxidase (ACO)* genes used in Figure 5C, eleven genes used in Figure 6C and one *BETA-AMYLASE (BAM)* gene used in Figure 7B.

**Method S1** Quantification of sesquiterpene accumulation in *Petunia* pistils and emission from tube by GC-MS.

Samples were analyzed on an Agilent 9000 Intuvo gas chromatograph system (Agilent Technologies), connected to an Agilent 5977B mass detector (Agilent Technologies). 2  $\mu$ L of samples were injected in a split/splitless injector set at 250 °C with a 2-fold split. Temperature of the guard chip was set to 75 °C at the beginning of the run before following the temperature of the oven in track oven mode. Bus temperature was set at 280 °C. Samples were analyzed on a HP-5MS-UI column (30 m x 0.25 mm x 0.25  $\mu$ m) (Agilent Technologies) using a program consisting of 1 min at 50 °C, followed by 20 °C.min<sup>-1</sup> to 310 °C, then 4 min at 310 °C, with helium as carrier gas set at 1.2 mL.min<sup>-1</sup>. Detector was set at 250 °C, ionization energy was set at 70 eV and analysis was realized in scan mode for analysis of sesquiterpene accumulation in pistils (Mass spectra scanned from 30 to 300 amu) and in single ion monitoring mode for analysis of sesquiterpene emission from tubes using m/z 161 to quantify sesquiterpenes and m/z 95 to quantify IS. Products were identified based on their retention times and electron ionization mass spectra compared to those of authentic standards (Germacrene D) or those present in the NIST2017 and WILEY libraries. Quantification of compounds was performed using the Mass Hunter quantitative software (Agilent Technologies) using response factors of authentic germacrene D relative to the IS and normalized to the weight of tissues.

**Method S2** Carotenoid extraction and quantification with an HPLC system.

Tissues were ground using a ball mill (Retch MM400, Retch). Extraction was performed for 15 min in microcentrifuge tubes containing 400  $\mu$ l 80% acetone in darkness under slight agitation (50 rpm). After this, samples were centrifuged in a microcentrifuge for 7 min at max speed. 100  $\mu$ l of the supernatant was transferred to an HPLC tube with insert. Pigments were separated with a YMC carotenoid S-5  $\mu$ m column (250 x 2.1 mm; YMC Europe GmbH). Pigments were eluted using 100% solvent A (Methanol: Methyl tert-butyl ether: H<sub>2</sub>O, 90:6:4) for the first 12 min followed by an 84 min linear gradient to 100% solvent B (MeOH/MTBE/H<sub>2</sub>O (25:71:4)). The column temperature was 35 °C, the flow rate 0.2 ml/min. The pigments were detected by their absorbance at 480 nm. Standards were used to identify carotenoids.

**Method S3** Starch extraction and quantification with an HPLC system.

After extraction, tubes were centrifuged at 25k x g for 5 min. For starch quantitation, the pellet was washed three times with 80% ethanol. The pellet was vacuum dried, and starch was catalyzed to glucose by a 2-step enzymatic reaction. For the first step, the pellet was resuspended in 0.8 mL  $\alpha$ -amylase solution (1 mg/ml in water, Rohalase® A3 from *Bacillus subtilis*, 44 U/mg, Serva) and incubated for 30 min at 90 °C while agitating. Subsequently, 0.4 ml amyglucosidase solution (0.5 mg/ml in 50 mM citrate buffer, pH 4.6, from *Aspergillus Niger*, 70U/mg, Sigma) was added, shortly mixed by vortex, and incubated for 10 min at 60 °C under agitation. Finally, samples were centrifuged, the supernatant was transferred to a new tube and diluted 20-fold. Glucose levels were analyzed with the HPLC, as described in **Method S2**, this time eluted with 100 mM NaOH + 25 mM sodium acetate instead of only 100 mM NaOH.